Cell Reports

Report

A Modular Differentiation System Maps Multiple Human Kidney Lineages from Pluripotent Stem Cells

Graphical Abstract

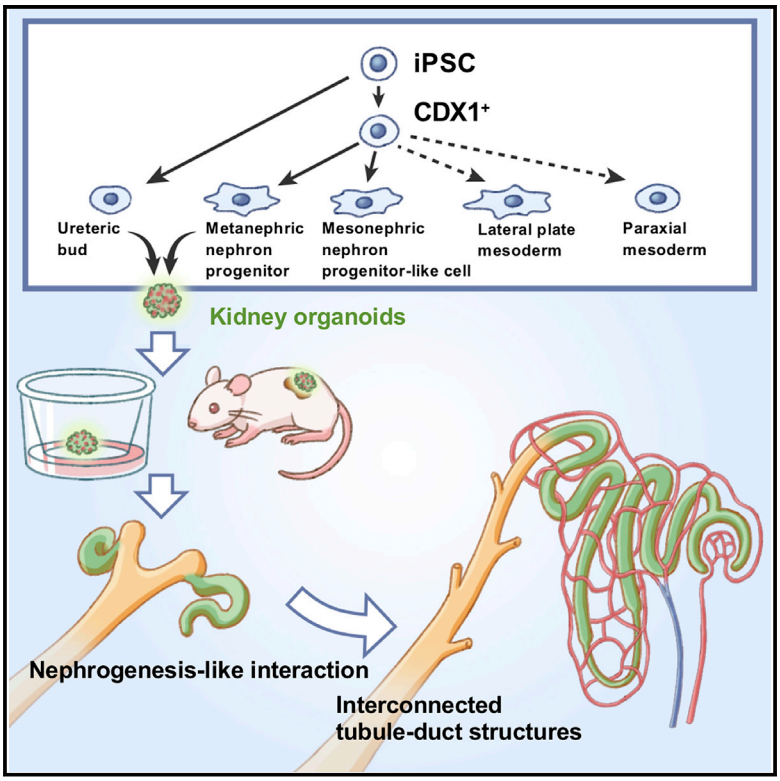

Highlights

- A 2D differentiation system for multiple mesoderm lineages is established
- Three different kidney progenitors separately induced from intermediate mesoderm
- hiPSC-derived metanephric progenitors and ureteric bud recapitulate nephrogenic niches
- hiPSC-derived progenitors and ureteric bud generate interconnected kidney organoids

Authors

Hiraku Tsujimoto, Tomoko Kasahara, Shin-ichi Sueta, ..., Makoto Ikeya, Akira Watanabe, Kenji Osafune

Correspondence

osafu@cira.kyoto-u.ac.jp

In Brief

Tsujimoto et al. establish a differentiation system that separately generates multiple mesoderm lineages from hiPSCs. Three kidney progenitors, metanephric nephron progenitors (NPs), mesonephric NP-like cells, and the ureteric bud (UB), are further induced. They also generate interconnected kidney organoids from separately induced metanephric NPs and UB.

Tsujimoto et al., 2020, Cell Reports *31*, 107476
April 7, 2020
https://doi.org/10.1016/j.celrep.2020.03.040

CellPress

Cell Reports
Report

A Modular Differentiation System Maps Multiple Human Kidney Lineages from Pluripotent Stem Cells

Hiraku Tsujimoto,[1,5] Tomoko Kasahara,[1,5] Shin-ichi Sueta,[1,5] Toshikazu Araoka,[1] Satoko Sakamoto,[1] Chihiro Okada,[1,2] Shin-ichi Mae,[1] Taiki Nakajima,[1] Natsumi Okamoto,[1] Daisuke Taura,[3] Makoto Nasu,[1] Tatsuya Shimizu,[1] Makoto Ryosaka,[1] Zhongwei Li,[4] Masakatsu Sone,[3] Makoto Ikeya,[1] Akira Watanabe,[1] and Kenji Osafune[1,6,*]

[1]Center for iPS Cell Research and Application (CiRA), Kyoto University, 53 Kawahara-cho, Shogoin, Sakyo-ku, Kyoto 606-8507, Japan
[2]Mitsubishi Space Software, 5-4-36 Tsukaguchi-honmachi, Amagasaki, Hyogo 661-0001, Japan
[3]Department of Medicine and Clinical Science, Kyoto University Graduate School of Medicine, 54 Kawahara-cho, Shogoin, Sakyo-ku, Kyoto 606-8507, Japan
[4]Department of Stem Cell Biology and Regenerative Medicine, Keck School of Medicine, University of Southern California, 1333 San Pablo Street, MMR 618, Los Angeles, CA 90033, USA
[5]These authors contributed equally
[6]Lead Contact
*Correspondence: osafu@cira.kyoto-u.ac.jp
https://doi.org/10.1016/j.celrep.2020.03.040

SUMMARY

Recent studies using human pluripotent stem cells (hPSCs) have developed protocols to induce kidney-lineage cells and reconstruct kidney organoids. However, the separate generation of metanephric nephron progenitors (NPs), mesonephric NPs, and ureteric bud (UB) cells, which constitute embryonic kidneys, in *in vitro* differentiation culture systems has not been fully investigated. Here, we create a culture system in which these mesoderm-like cell types and paraxial and lateral plate mesoderm-like cells are separately generated from hPSCs. We recapitulate nephrogenic niches from separately induced metanephric NP-like and UB-like cells, which are subsequently differentiated into glomeruli, renal tubules, and collecting ducts *in vitro* and further vascularized *in vivo*. Our selective differentiation protocols should contribute to understanding the mechanisms underlying human kidney development and disease and also supply cell sources for regenerative therapies.

INTRODUCTION

In amniotes, the mesonephros is the embryonic kidney, and the more complex metanephros acts as the adult kidney. The mammalian metanephros develops by mutual interactions between two progenitor tissues, the ureteric bud (UB) and the metanephric mesenchyme (MM) (Costantini and Kopan, 2010; Taguchi et al., 2014). Several groups including ours have reported induction protocols for kidney progenitor cells from human pluripotent stem cells (hPSCs) (Mae et al., 2018; Morizane et al., 2015; Taguchi et al., 2014; Taguchi and Nishinakamura, 2017; Takasato et al., 2014, 2015; Toyohara et al., 2015; Xia et al., 2013). Taguchi et al. (2014) found that inducing axial stem cells and the posterior intermediate mesoderm (IM) could facilitate the derivation of metanephric nephron progenitors (NPs) by using an embryoid body culture system. Morizane et al. (2015) induced metanephric NPs at high efficiency in two-dimensional (2D) cultures. Takasato et al. (2015) have generated kidney organoids by simultaneously inducing MM and UB lineages. Taguchi and Nishinakamura (2017) succeeded in generating UB cells through anterior IM from mouse embryonic stem cells (mESCs) and human induced pluripotent stem cells (hiPSCs). The induced mouse UB cells showed branching morphogenesis and generated interconnection between NP-derived nephrons and UB-derived collecting ducts. However, the separate generation of metanephric NPs, mesonephric NPs, and UB cells in *in vitro* differentiation culture systems or the recapitulation of nephrogenesis-like physiological interactions between metanephric NPs and UB cells that occur in embryonic kidneys has not been fully investigated. Furthermore, the reconstruction of kidney structures, in which separately induced hPSC-derived metanephric NPs and UB cells are interconnected, has not been achieved.

In this study, we established a differentiation culture system that provides a roadmap to inducing multiple progenitors constituting embryonic kidneys. Using this system, we recapitulated nephrogenesis-like interactions between metanephric NPs and UB cells, which subsequently generated glomeruli and interconnected renal tubules and collecting ducts *in vitro* and *in vivo*.

RESULTS

Induction of hiPSCs into CDX1$^+$ Cells Committed to Mesoderm

The formation of the primitive streak (PS) is the first step in mesoderm development. To induce mesoderm from PSCs, we tested various concentrations of a glycogen synthase kinase 3β (GSK-3β) inhibitor, CHIR99021, which is a key regulator of mesoderm induction, and monitored the expression of a PS marker, BRACHYURY, on an hiPSC line, 585A1 (Evans et al., 2012; Mendjan et al., 2014; Okita et al., 2013). Immunofluorescence analysis showed that >3 μM CHIR99021 induced BRACHYURY$^+$ PS cells (Figure 1A).

According to chick development, CDX1$^+$ epiblast cells are committed to mesodermal cells (Meyer and Gruss, 1993). We

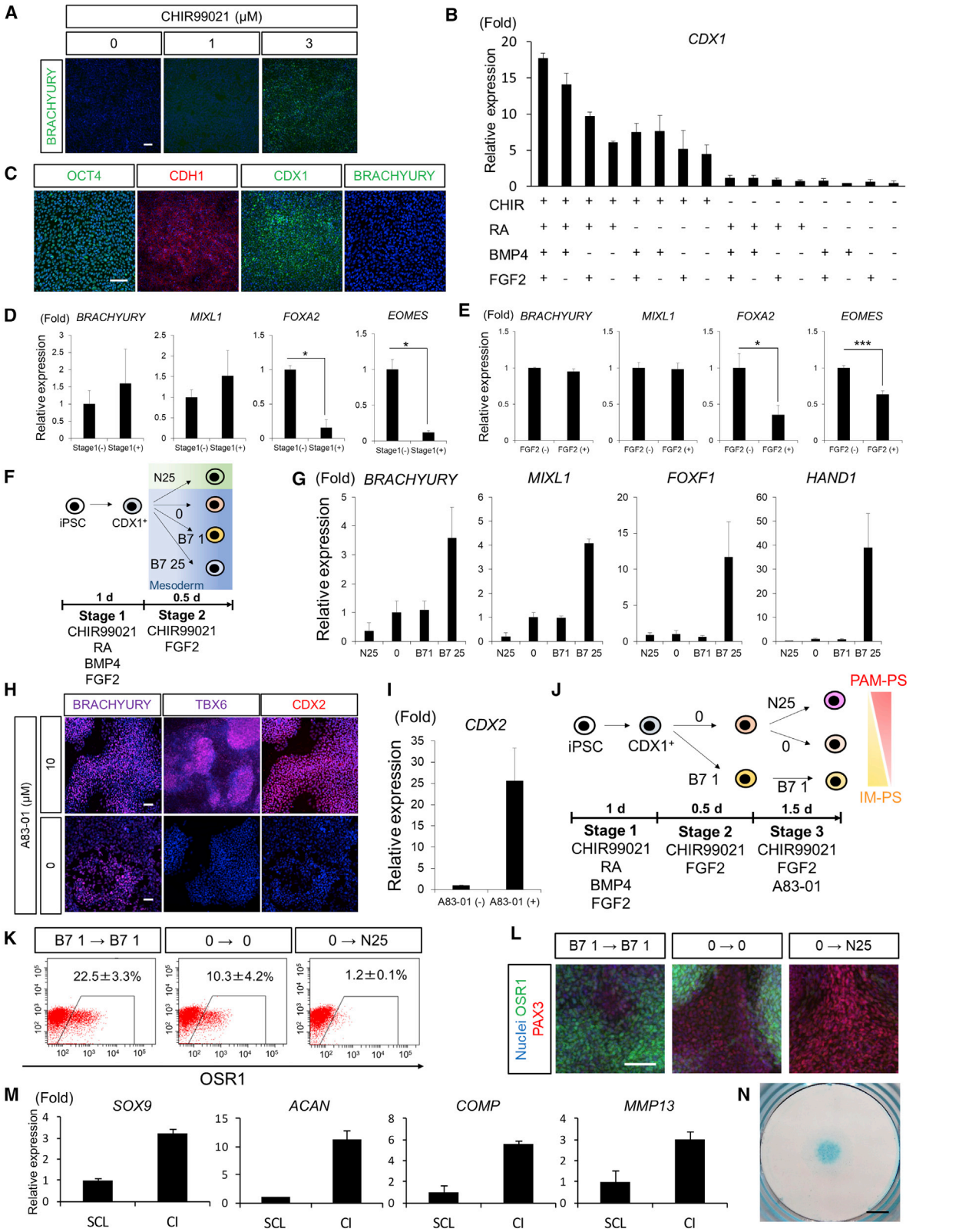

(legend on next page)

confirmed that treatment with 1 μM CHIR99021, 10 nM retinoic acid (RA), 1 ng/mL bone morphogenetic protein (BMP) 4, and 100 ng/mL fibroblast growth factor (FGF) 2 induced hiPSCs to differentiate into CDX1$^+$ cells. These four factors had previously been shown to relate to the expression of CDX1 in the epiblast stage (Houle et al., 2003; Keenan et al., 2006; Lengerke et al., 2008). We generated CDX1$^+$ cells within 24 h of hiPSC differentiation by activating the four signaling pathways (Figure 1B). As expected, the induced CDX1$^+$ cells also expressed a pluripotent marker, OCT4, and an epithelial marker, CDH1, but not BRACHYURY (Figure 1C), suggesting that the induced CDX1$^+$ cells have epiblast-like characteristics.

Next, we evaluated the effects of adding the CDX1$^+$ cell induction stage (stage 1) before the PS induction process on the expression of mesodermal and endodermal markers. qRT-PCR analyses showed that although PS induction protocols with or without stage 1 successfully induced BRACHYURY$^+$ PS cells, the inclusion of stage 1 significantly downregulated the endodermal genes *FOXA2* and *EOMES* (Figure 1D). Therefore, the addition of stage 1 prevented differentiation into endoderm-committed PS. A previous study also showed that blocking FGF signaling increased endodermal cell mass in amphibian animal cap explants (Cha et al., 2004). We therefore addressed the effects of adding FGF2 to the CHIR99021 treatment at the PS induction stage (stage 2). We found that the activation of FGF signaling blocked endoderm formation but maintained PS induction (Figure 1E). These results indicate that we established a protocol that induces hiPSCs through CDX1$^+$ cells into mesoderm-committed PS cells.

Induction of Lateral Plate Mesoderm

BMP signaling induces the formation of posterior PS and represses anterior PS lineage, thus driving the bifurcation of these two PS subtypes in vertebrates (Faial et al., 2015). In addition, BMP7 is a main player among BMP signals in vertebrate PS formation (Streit et al., 1998). We thus attempted to generate PS subtypes by adding a BMP signaling gradient in the first 12 h of stage 2 (Figures 1F and 1G). CDX1$^+$ cells treated with 25 ng/mL BMP7 (moderate concentration) for 12 h expressed the posterior PS markers *FOXF1* and *HAND1* in addition to *BRACHYURY* and *MIXL1*. Blocking BMP signaling by treatment with 25 ng/mL NOGGIN abrogated PS induction (Figure 1G).

In vertebrate embryos, posterior PS gives rise to lateral plate mesoderm (LPM) cells, and vascular endothelial cells (ECs) are derived from an LPM subpopulation (Zhong et al., 2001). Previous studies have emphasized the critical role of BMP signaling in the differentiation of hPSCs toward LPM cells (Iyer et al., 2016; Mendjan et al., 2014). We thus prolonged the 25 ng/mL BMP7 treatment at stage 2 and found that FLK1$^+$ LPM cells were generated at an induction rate of 96.8% ± 0.5% (n = 3) on stage 2, day 3 (Figure S1A). We next aimed to drive these progenitors toward ECs by using vascular specification media at stage 3 (James et al., 2010; Nguyen et al., 2016). Because WNT-β-catenin signaling induces endothelial mesenchymal transformation and may inhibit EC formation (Kovacic et al., 2012), we added IWR-1, an inhibitor of the WNT-β-catenin pathway, to the directed differentiation protocol (Figure S1B). Flow cytometric analysis of hiPSC-derived cells on stage 3, day 4 showed that >90% of cells were vascular endothelial (VE)-cadherin$^+$. Consistently, both RT-PCR and immunofluorescence analyses showed that stage 3, day 4 cells without purification expressed substantially higher levels of the EC markers CD31 and eNOS (Figures S1C and S1D). Next, we carried out a tube formation assay to confirm the angiogenic potential of our hiPSC-derived ECs (Figure S1E). We confirmed the robustness of our differentiation protocol on 4A6, which is an OSR1-GFP/SIX2-tdTomato reporter hiPSC line generated from 201B7 (Figures S1F and S1G) (Mae et al., 2013; Toyohara et al., 2015). We also confirmed that our differentiation protocol was applicable under feeder-free cultures (Figure S1H). These results

Figure 1. Differentiation from hiPSCs through CDX1$^+$ Epiblast-like Cells into LPM- and PAM-PS Cells

(A) Immunostaining analyses for BRACHYURY after 24 h treatment of hiPSCs with 0 (DMSO), 1, or 3 μM CHIR99021.

(B) qRT-PCR analysis of *CDX1* expression after 24 h treatment of hiPSCs with various combinations of 4 factors. Each value was normalized to that of hiPSCs.

(C) Immunostaining analyses for OCT4, CDH1, CDX1, and BRACHYURY after 24 h treatment with the 4 factors.

(D) qRT-PCR analysis shows that the addition of the CDX1$^+$ cell induction step (stage 1) significantly downregulates endodermal gene expression. Each value was normalized to that of stage 2 cells treated without the CDX1$^+$ stage.

(E) qRT-PCR analysis shows that the addition of FGF2 significantly downregulates endodermal gene expression. Each value was normalized to that of stage 2 cells without FGF2 treatment.(F) A simplified scheme of mesoderm induction and patterning defined by signaling gradients in distinct regions of PS.

(G) qRT-PCR analyses of mesodermal and endodermal gene expressions after treating CDX1$^+$ cells for 24 h with the indicated concentrations of BMP7 or a BMP inhibitor, NOGGIN, at the PS induction stage (stage 2). N25, 25 ng/mL NOGGIN; B7 1, 1 ng/mL BMP7; B7 25, 25 ng/mL BMP7. Each value was normalized to that of stage 2 cells treated without any additional factors.

(H) Immunostaining analyses for BRACHYURY, TBX6, and CDX2 in CDX1$^+$ cells treated with 3 μM CHIR99021 and 100 ng/mL FGF2 for 24 h and then with or without 10 μM A83-01 for an additional 2 days.

(I) qRT-PCR analysis for *CDX2* expression in CDX1$^+$ cells treated with 3 μM CHIR99021 and 100 ng/mL FGF2 for 24 h and then with or without 10 μM A83-01 for an additional 2 days. Each value was normalized to that of stage 3 cells without A83-01 treatment.

(J) A hypothetical scheme of mesoderm induction and patterning.

(K) Flow cytometric analyses of 4A6 treated with the indicated concentrations of BMP7 and NOGGIN at the PS and late-PS induction stages after an additional 3-day culture without any inducing factors.

(L) Late PS cells treated with a low BMP7 expressed OSR1 (LPM-IM marker), while NOGGIN-treated late PS cells expressed PAX3 (PAM marker), after an additional 3-day culture without any inducing factors.

(M) qRT-PCR analyses of marker expressions for sclerotome (SCL) and chondrogenic induction (CI). Each value was normalized to that of sclerotome cells.

(N) Cartilage tissue differentiated from PAM through somitic mesoderm and sclerotome, as analyzed by Alcian blue staining.

*$p < 0.05$ and ***$p < 0.001$ by Student's t test in (D) and (E). The data from 3 independent experiments are presented as the means ± SEMs (n = 3) in (B), (D), (E), (G), (I), and (M). Scale bars, 100 μm in (A), (C), (H), and (L) and 200 μm in (N).

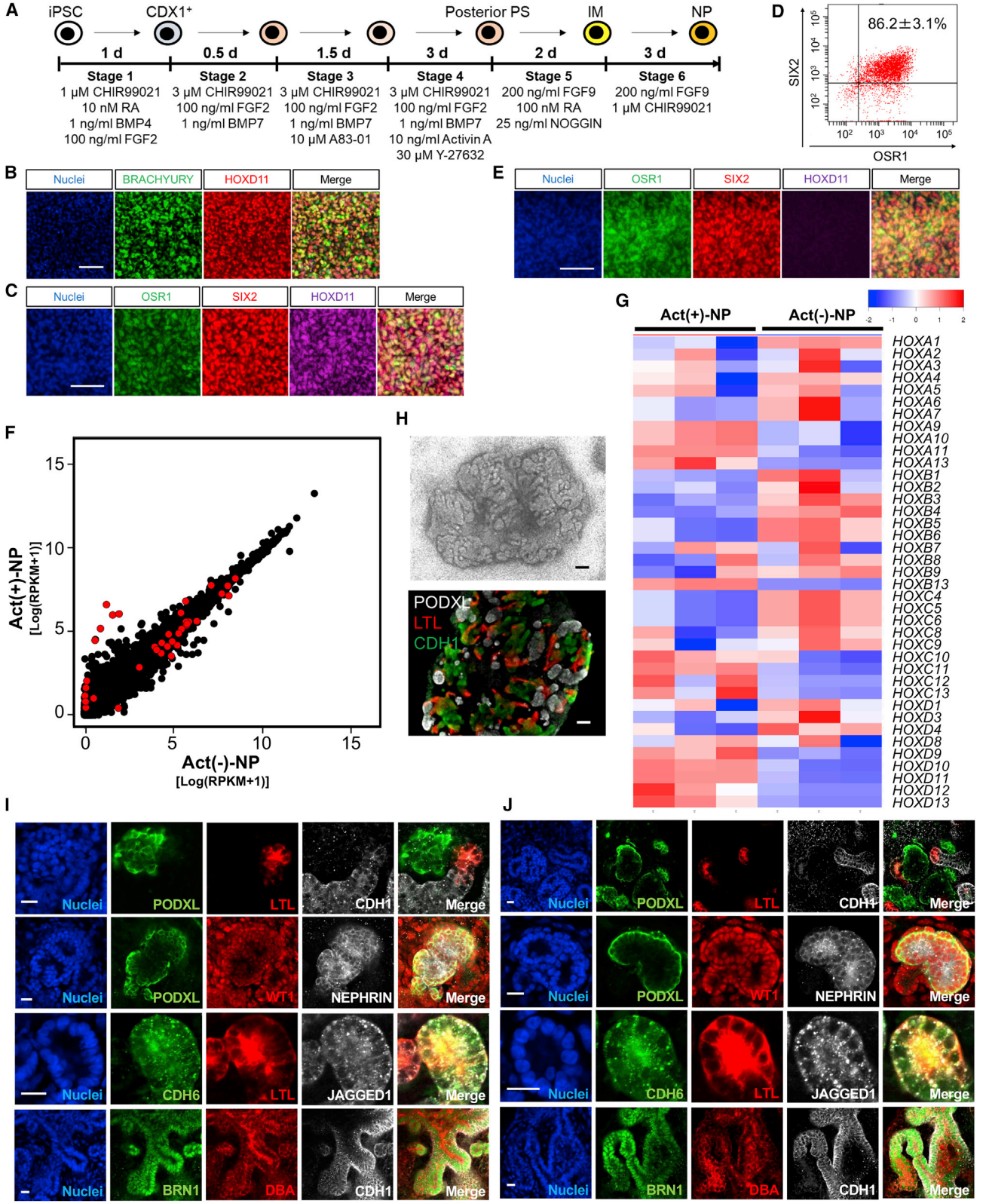

(legend on next page)

indicate that vascular ECs can be robustly generated by our differentiation protocol through PS committed to LPM cells (Figures S8A and S8B [i]).

Smad2/3 Inhibition after PS Induction Stage Induces Late PS

Based on our qRT-PCR data (Figures 1F and 1G), we hypothesized that the PS induction stage (stage 2) with or without low-dose BMP (1 ng/mL) may induce paraxial mesoderm-committed PS (PAM-PS) or IM-committed PS (IM-PS) cells. Previous studies induced caudal PAM and NPs from hPSCs via BRACHYURY$^+$CDX2$^+$ late PS cells (Mendjan et al., 2014; Morizane et al., 2015; Taguchi et al., 2014; Takasato et al., 2015). Because Smad2/3-related signals are crucial for repressing CDX2 expression in hPSC differentiation (Sakaki-Yumoto et al., 2013), we hypothesized that an ALK5 inhibitor, A83-01, may facilitate CDX2$^+$ late PS cell induction. To confirm this hypothesis, we induced BRACHYURY$^+$ PS cells from CDX1$^+$ cells with CHIR99021 and FGF2 for 12 h at stage 2 and then treated the cells with A83-01 (Figure 1H). At stage 3, the expressions of BRACHYURY, TBX6, and CDX2, which represent a nascent posterior mesoderm, were upregulated (Figures 1H and 1I). Therefore, our differentiation protocol was able to induce late PS cells toward caudal PAM and NPs.

Induction of PAM from Late PS Cells

Next, we aimed to induce PAM-PS and IM-PS cells from our late PS cells. To monitor the induction of PAM-PS and IM-PS cells, we used 4A6. We found that the PS induction stage (stage 2) without BMP treatment reduced the induction of cells positive for an IM-LPM marker gene, OSR1, and the addition of NOGGIN at the late PS induction stage (stage 3) further repressed the induction (Figures 1J–1L). We investigated the expression of *OSR1*, the LPM marker *HAND1*, and the PAM markers *PARAXIS*, *MEOX1*, and *PAX3* with various BMP signaling treatments at stages 2 and 3 (Figure S1I). Treatments with moderate or low concentrations of BMP7 at stages 2 and 3 upregulated the expressions of *OSR1* and *HAND1* or *OSR1* alone, indicating that the two treatments induced LPM and IM, respectively. Treatment without BMP at stage 2 and with NOGGIN at stage 3 induced the expression of PAM marker genes (Figures 1L, S1J, and S1K). We next examined the somitic lineage differentiation capacity of the NOGGIN-treated late PS cells by using a sclerotome and cartilage induction protocol (Nakajima et al., 2018) and found that the cells sequentially expressed markers for presomitic and somitic mesoderm, sclerotome, and cartilage (Figures 1M, S1K, and S1L). The formation of cartilage tissue was confirmed by Alcian blue staining (Figure 1N). These results suggest that our method can induce late PS cells to PAM-PS cells (Figures S8A and S8B [ii]).

Induction of Kidney Lineage Progenitors from Late PS Cells

We found that adding a low concentration of BMP7 at stages 2 and 3 favors IM gene expression (Figures 1J–1L and S1I). Next, we aimed to induce metanephric NPs from late PS cells (Figure 2A). Since the activation of transforming growth factor β (TGF-β) signaling through the Gdf11-activin receptor IIA and IIB (AcrIIA, AcrIIB) enhances the transcriptional activation of *Hoxd11*, which regulates the posterior specification for metanephros development (Gaunt et al., 2013; Oh et al., 2002), we examined whether activin A, an agonist of activin receptors, induced metanephric NPs with HOXD11 expression. Immunocytochemistry showed that exposing late PS cells to activin A induced HOXD11 expression, indicating that activin A contributed to terminal patterning (Figure 2B). We then generated IM by adding FGF9, RA, and a BMP signaling inhibitor, NOGGIN, at stage 5, followed by inducing NPs with FGF9 and CHIR99021 at stage 6 (Morizane et al., 2015; Taguchi et al., 2014; Takasato et al., 2015) (Figure 2A). We confirmed the expression of nephrogenic genes during stage 5 for IM induction and further gene activation after stage 6 culture, producing NP cells (Figure S2A). Our differentiation method generated OSR1$^+$SIX2$^+$ cells at >85% induction efficiency from 4A6 (Figures 2C and 2D) and was also applicable to 585A1 maintained on feeder cells (Figure S2B). Furthermore, our method was applicable to feeder-free cultures by adjusting the concentration of CHIR99021 from stages 2–4 and the duration of stage 2 (Figure S2C). Two additional hiPSC lines under feeder-free culture conditions, 585A1 and CiRA00009, the latter of which is an hiPSC line derived from a patient with autosomal dominant polycystic kidney disease (Ameku et al., 2016), were efficiently induced into SIX2$^+$ cells at efficiencies of 76.1% ± 3.2% (n = 3) and 69.2% ± 4.9% (n = 3), respectively (Figure S2D). These results were confirmed by qRT-PCR for *SIX2* and *CITED1* (Figure S2E).

Although SIX2$^+$ cells induced without activin A treatment at stage 4 exhibited low HOXD11 expression, we unexpectedly observed that PS cells unexposed to activin A could differentiate into cells expressing the NP markers OSR1 and SIX2 at an

Figure 2. Differentiation into Nephron Progenitor Cells and Formation of 3D Nephron Structures

(A) Differentiation protocol for HOXD11$^+$ IM cells and NPs.

(B) Immunostaining analyses of BRACHYURY$^+$HOXD11$^+$ late PS cells on stage 4, day 3.

(C) Immunostaining analyses of NP-like cells induced with activin A treatment at stage 4 (Act(+)-NPs) on stage 6, day 3.

(D) Flow cytometric analysis of Act(+)-NPs for OSR1 and SIX2 expression on stage 6, day 3.

(E) Immunostaining analyses of NP-like cells induced without activin A treatment at stage 4 (Act(−)-NPs) on stage 6, day 3.

(F) Dot plots showing gene expressions in Act(+)- and Act(−)-NPs. Red dots show *HOX* cluster genes.

(G) Heatmap showing the expression levels of *HOX* cluster genes determined by RNA-seq.

(H) Bright-field (top panel) and immunofluorescence (bottom panel) images of aggregates formed from Act(+)-NPs after 10 days of air-liquid interface cultures. CDH1, distal tubule marker cadherin 1 (green); LTL, proximal tubule marker *Lotus tetragonolobus* lectin (red); PODXL, podocyte marker podocalyxin (white).

(I and J) Whole-mount immunofluorescence analyses of day 10 nephron structures formed from Act(+)-NPs (I) and Act(−)-NPs (J) for markers of glomerular podocytes and proximal and distal renal tubules.

Scale bars, 100 μm in (B), (C), (E), and (H) and 20 μm in (I) and (J).

induction efficiency of 34.2% ± 2.5% (n = 3; Figures 2E, S2F, and S2G). To address differences between NP-like cells induced with and without activin A treatment (Act(+)-NP and Act(−)-NP, respectively), we conducted RNA sequencing (RNA-seq). Although the gene expression profiles of the two cell types were similar, differentially expressed genes were detected (Tables S1 and S2). In particular, we found a major difference in the expression of *HOX* genes (Figures 2F and 2G); Act(+)-NPs had a high expression of *HOXD11*, but Act(−)-NPs did not upregulate posterior *HOX* genes (Figure 2G). Single-cell RNA-seq analyses showed that both Act(+)-NP and Act(−)-NP populations were transcriptionally close to the NP population in gestational week (GW) 16 fetal human kidneys (Figure S3A; Lindström et al., 2018b).

We then examined the developmental potential of Act(+)-NPs to reconstitute 3D nephron-like structures *in vitro* by using a previously reported air-liquid interface culture method (Li et al., 2016). Histological analysis showed nephron-constituting segments, including glomeruli and proximal and distal tubules, contiguously connected to the nephron structures (Figures 2H and 2I). Notably, reconstructed 3D organoids made from Act(−)-NPs also developed glomeruli- and proximal and distal tubule-like structures (Figures 2J and S2H), but the expression of two Henle's loop markers, *UMOD* and *NKCC2*, was significantly lower in the organoids derived from Act(−)-NPs than in those from Act(+)-NPs (Figure S2I), implying that Act(−)-NPs were progenitors of mesonephros, because mammalian mesonephros lacks Henle's loop (Wintour et al., 1996). Although RNA-seq analysis did not show large differences in the gene expression profiles between the two organoids (Figure S2J), hierarchical clustering of the gene expression profiles of the organoids generated from Act(+)-NPs indicated similarity with the fetal human kidney of the first and second trimesters of pregnancy (Figure S3B; Takasato et al., 2015). Another study reported markers for mouse mesonephros, including markers for early Henle's loop (Georgas et al., 2011). Consistently, our RNA-seq data showed the significant upregulation of several mesonephros markers (*TCN2*, *FBP1*, *SLC27A2*, and *ENTPD5*) and of early Henle's loop (*AADAC* and *GPD1*) in the organoids generated from Act(−)-NPs compared with Act(−)-NPs (Figure S3C).

The different origins of mesonephros and metanephros occur as distinct temporal sequences in the anterior-posterior axis (Mugford et al., 2008; Taguchi et al., 2014). Our Act(−)-NPs featured the expression of anterior HOX genes, whereas HOXD11 expression was higher in Act(+)-NPs, further suggesting that Act(−)-NP cells represent the anterior NP-like cells that generate mesonephros (Figure 2G). In embryonic day (E) 11 mice, a higher expression of integrin α8 (Itga8) was reported in mesenchymal cells throughout the nephrogenic cord, which include mesonephric NPs, than in metanephric NPs (Figure S2K; Müller et al., 1997). Consistently, Act(−)-NPs had a higher expression of ITGA8 than did Act(+)-NPs (Table S1). These data suggest that Act(+)-NPs correspond to the metanephric NPs of fetal kidney and that Act−)-NPs are mesonephric NP-like cells, indicating the successful induction of late PS and IM-PS cells with developmental potential to differentiate into these two NPs and the generation of 3D nephron-like structures from hiPSCs (Figures S8A and S8B [iii], [iv]).

Finally, we attempted to generate UB lineages. We recently established a directed differentiation protocol of UB cells from hiPSCs by mimicking mammalian UB development *in vivo*, which includes stepwise differentiation through anterior PS, anterior IM, and Wolffian duct (WD) stages (Mae et al., 2018). We aimed to modify the UB induction protocol by adding the $CDX1^+$ cell step and using the culture conditions established in this study. Adding the $CDX1^+$ cell step in advance of the anterior PS induction stage prevented differentiation to UB lineage (Figure S4A). We instead found that branching UB structures were successfully generated from $CDX1^-$ cells in our culture system (Figures S4B, S4C, S8A, and S8B [v]). These results suggest that UB cells may have different origins at the epiblast stage from metanephric and mesonephric NPs.

hiPSC-Derived Metanephric NPs and UB Cells Interact and Recapitulate Nephrogenesis *In Vitro*

Next, we aimed to reconstruct kidney structures from our hiPSC-derived metanephric NPs and UB cells. For this purpose, we used 201B7-derived hiPSC lines constitutively expressing GFP (317-12) or mCherry (511-3E; Oceguera-Yanez et al., 2016) and 2 hiPSC lines without fluorescent reporters (585A1 and 1231A3), which allowed us to distinguish the lineage of NP and UB cell-derived tissues in co-culture experiments. We adopted the *in vitro* organ culture system, in which culture media containing high concentrations of KnockOut Serum Replacement (KSR) and plate agitation by a seesaw shaker were used to achieve better survival of the cell aggregates (Przepiorski et al., 2018).

It was reported that in the mixed cultures of dissociated NPs and UB cells from mouse embryos, UB cells first self-organize by themselves and then start mutual interaction with NPs (Lefevre et al., 2017). We accordingly dissociated and mixed the hiPSC-derived NPs and UB cells to promote cell-to-cell contacts and interactions (Figure 3A). Consistent with the findings of mouse embryos, single UB cells from 1231A3 constructed $CALB1^+$ or $CK8^+$ epithelia that were surrounded by 317-12-derived GFP^+SIX2^+ or GFP^+WT1^+ NPs on day 4, which is reminiscent of nephrogenic niches in mouse embryos (Figures 3B and S5A). This result was reproduced in $tdTomato^+$ NPs differentiated from 4A6- and 1231A3-derived UB cells (Figure 3C). A recent study investigating human embryonic kidneys indicated transcription factor SIX1 as a specific marker for human NPs during active nephrogenesis (Lindström et al., 2018b). Another report demonstrated that $LEF1^+$ NPs exist near the ureteric tip and develop pre-tubular aggregates and renal vesicles in humans, and that the connecting and distal segments of human S-shaped bodies are $JAGGED1^-HNF1B^+$, while the medial and proximal segments are $JAGGED1^+HNF1B^+$ (Lindström et al., 2018c). As expected, GFP^+SIX1^+ and GFP^+SALL1^+ cells constituted cap mesenchyme-like structures localized near $CALB1^+RET^+$ UB tip-like structures, and GFP^+LEF1^+ cells were localized near UB tip- and renal vesicle-like structures in the co-culture of 317-12-derived NPs and 585A1 or 1231A3-derived UB cells on day 6 (Figures 3D and S5B). We also found that the distal parts of GFP^+BRN1^+ and GFP^+HNF1B^+ S-shaped body-like structures, whose proximal or medial parts were $JAGGED1^+$, were connected to $CALB1^+$ or $CK8^+$ UB tip-like structures (Figures 3E and S5C). GFP^+MAFB^+ podocyte progenitors were

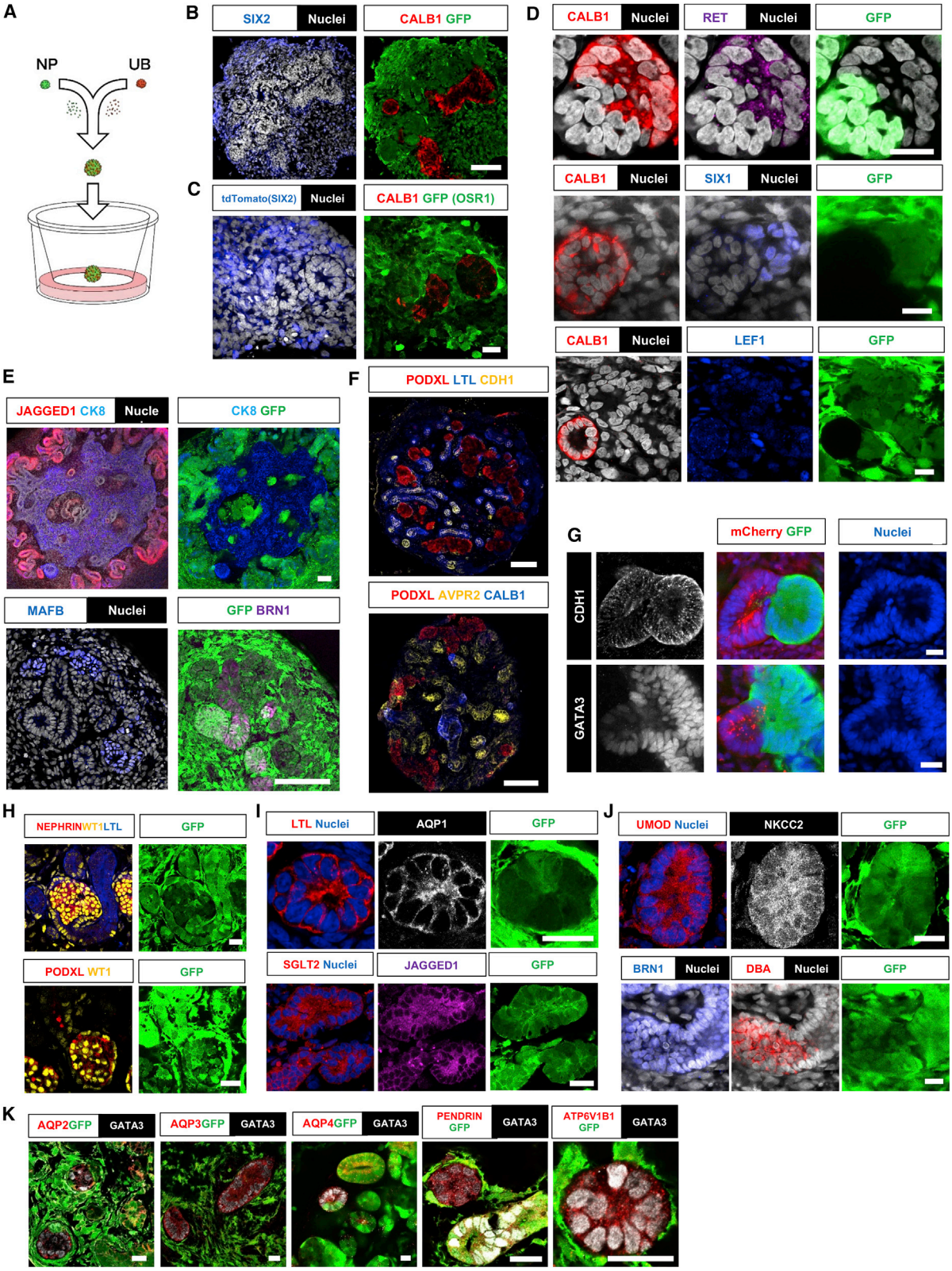

(legend on next page)

observed at the proximal end of the S-shaped body-like structures (Figure 3E).

In embryonic kidneys, UB cells secrete Wnt11 in response to glial cell-derived neurotrophic factor (GDNF) secreted by NPs and maintain the expression of Ret and its downstream targets, Etv4 and Etv5 (Lu et al., 2009). In mice, Elf3 is expressed in collecting duct principal cells and increases the expression of Aqp2 and Avpr2 (Grassmeyer et al., 2017). We thus generated kidney organoids from 317-12-derived NPs and 511-3E-derived UB cells and examined the expression of the aforementioned molecules in UB cells isolated by flow cytometry on day 10 (Figures S5D–S5G). As expected, the expression of *RET* and of markers for the UB trunk (*WNT7B* and *TACSTD2*) was maintained, while the expression of *ETV4* and *ETV5* and of markers for the collecting duct (*AVPR2*, *AQP3*, *KLF5*, *ELF3*, and *ATP6V1B1*) was significantly upregulated in UB-derived cells upon co-culture compared with before co-culture or culture without NPs for 10 days (Figures S4B and S5D–S5G; Table S3; Wang et al., 2018). Furthermore, the co-culture of hiPSC-derived NPs and UB cells resulted in differentiation into kidney structures, while the culture of hiPSC-derived NPs alone did not (Figures S5H and S5I). These results suggest that our hiPSC-derived metanephric NPs and UB cells approximately show the reciprocal interactions seen by their counterparts in embryonic kidneys.

hiPSC-Derived Metanephric NPs and UB Cells Reconstruct Interconnected Kidney Structures *In Vitro*

By culture day 20, the organoids from 317-12-derived GFP$^+$ NPs and 1231A3-derived UB cells developed kidney structures containing PODXL$^+$ podocytes, LTL$^+$ proximal tubules, CDH1$^+$ or AVPR2$^+$ distal tubules and collecting ducts, and CALB1$^+$ collecting ducts (Figure 3F). We then examined epithelial connections in the organoids generated from 317-12-derived GFP$^+$ NPs and 511-3E-derived mCherry$^+$ UB cells and confirmed connections between GFP$^+$ tubular structures and mCherry$^+$ ductal structures by counterstaining with anti-CDH1, anti-GATA3, and anti-CK8 antibodies (Figures 3G and S6A). The connecting sites were positive for markers of distal tubules or collecting ducts (AQP2, AQP3, AQP4, PAX8, AVPR2, HNF1B, SOX9, and CK19) and for a marker of collecting ducts (CALB1) in the organoids from 317-12-derived GFP$^+$ NPs and 585A1- or 1231A3-derived UB cells, which is consistent with embryonic kidneys (Figures S6B–S6D; Harding et al., 2011; Lindström et al., 2018c). In the organoids, markers of glomerular podocytes (NEPHRIN, WT1, and PODXL; Figure 3H), proximal tubules (LTL, AQP1, SGLT2, JAGGED1, and CDH6; Figures 3H, 3I, and S6E), Henle's loop (UMOD, NKCC2, and BRN1; Figures 3J and S6F), and distal tubules (BRN1 and DBA; Figure 3J) were expressed in GFP$^+$ NP-derived structures. In contrast, we found GFP$^-$GATA3$^+$ collecting duct cells double positive for several principal cell markers (AQP2, AQP3, and AQP4) and two intercalated cell markers (PENDRIN and ATP6V1B1; Figures 3K and S6G; Chen et al., 2017). Unlike mice, human collecting ducts, but not distal tubules express CALB1 in GW8–11 developing kidneys (Lindström et al., 2018a). We also confirmed in GW28 human embryonic kidneys that only collecting ducts express CALB1, while both distal tubules and collecting ducts are positive for AQP2, AQP3, AQP4, BRN1, GATA3, CDH1, and DBA (Figures S7A–S7D). Consistently, while we did not detect CALB1 in tubules derived from GFP$^+$ metanephric NPs (Figures 3B–3D, S6C, and S6G), we found GFP$^+$ distal tubules positive for AQP2, AQP3, AQP4, BRN1, GATA3, CDH1, or DBA (Figures 3G, 3J, 3K, S6B–S6D, and S6G). These data suggest that hiPSC-derived NPs and UB cells reconstructed the kidney structures with interconnected renal tubules and collecting ducts *in vitro*.

hiPSC-Derived Metanephric NPs and UB Cells Reconstruct Interconnected and Vascularized Kidney Structures *In Vivo*

Finally, we transplanted mixed cellular aggregates of 317-12-derived GFP$^+$ NPs and 585A1- or 1231A3-derived UB cells under the kidney capsule of immunodeficient mice, as previously

Figure 3. *In Vitro* Reconstruction of Kidney Structures from Induced Metanephric NPs and UB Cells

(A) Schematic showing the *in vitro* reconstruction of kidney structures.

(B) Immunofluorescence analyses for SIX2 (NP marker) and CALB1 (UB marker) on a mixed aggregate of metanephric GFP$^+$ NP and GFP$^-$ UB cells on day 4 of the co-culture.

(C) Immunofluorescence analyses for tdTomato, GFP, and CALB1 on a mixed aggregate of metanephric NPs differentiated from 4A6 and GFP$^-$ UB cells on day 4 of the co-culture.

(D) Immunofluorescence analyses of day 6 organoids from GFP$^+$ NPs and GFP$^-$ UB cells show that the GFP$^-$CALB1$^+$RET$^+$ UB tip-like structure connected to the GFP$^+$ NP-derived structure (top panels) and that the GFP$^+$SIX1$^+$ cap mesenchyme-like structure (middle panels) and the GFP$^+$LEF1$^+$ NPs localized near GFP$^-$CALB1$^+$ UB tip-like structures (bottom panels).

(E) Immunofluorescence analyses of day 6 organoids from GFP$^+$ NPs and GFP$^-$ UB cells show that GFP$^+$ S-shaped body-like structures, whose proximal or medial parts were JAGGED1$^+$, connected to GFP$^-$CK8$^+$ UB tip-like structures (top panels) and that MAFB$^+$ podocyte progenitors localized at the proximal end of GFP$^+$ S-shaped body-like structures, whose medial and distal parts were BRN1$^+$ (bottom panels).

(F) Triple immunofluorescence analyses of day 20 organoids for markers of podocytes (PODXL), proximal tubules (LTL), and distal tubules or collecting ducts (CDH1; top panel), and for PODXL and markers of distal tubules or collecting ducts (AVPR2) and colleting ducts (CALB1; bottom panel). Note that weak CDH1 signals were also found in parts of the LTL$^+$ proximal tubules in the top panel.

(G) Immunofluorescence analyses of day 10 organoids derived from GFP$^+$ NPs and UB cells differentiated from hiPSCs constitutively expressing mCherry for markers of distal tubules or colleting ducts (CDH1 and GATA3).

(H–J) Immunofluorescence analyses of days 10–20 organoids derived from GFP$^+$ NPs and GFP$^-$ UB cells for markers of glomerular podocytes (NEPHRIN, WT1, and PODXL; H), proximal tubules (LTL, AQP1, SGLT2, and JAGGED1; H and I), Henle's loop (UMOD, NKCC2, and BRN1; J), and distal tubules (BRN1 and DBA; J).

(K) Immunofluorescence analyses of day 20 organoids derived from GFP$^+$ NPs and GFP$^-$ UB cells show GFP$^-$AQP2$^+$GATA3$^+$, GFP$^-$AQP3$^+$GATA3$^+$, and GFP$^-$AQP4$^+$GATA3$^+$ principal cells and GFP$^-$PENDRIN$^+$GATA3$^+$ and GFP$^-$ATP6V1B1$^+$GATA3$^+$ intercalated cells of collecting ducts. Note that GFP$^+$AQP2$^+$GATA3$^-$, GFP$^+$AQP4$^+$GATA3$^-$, and GFP$^+$PENDRIN$^+$GATA3$^+$ distal tubules were also found.

Scale bars, 100 μm in (B), (E), and (F) and 20 μm in (C), (D), and (G)–(K).

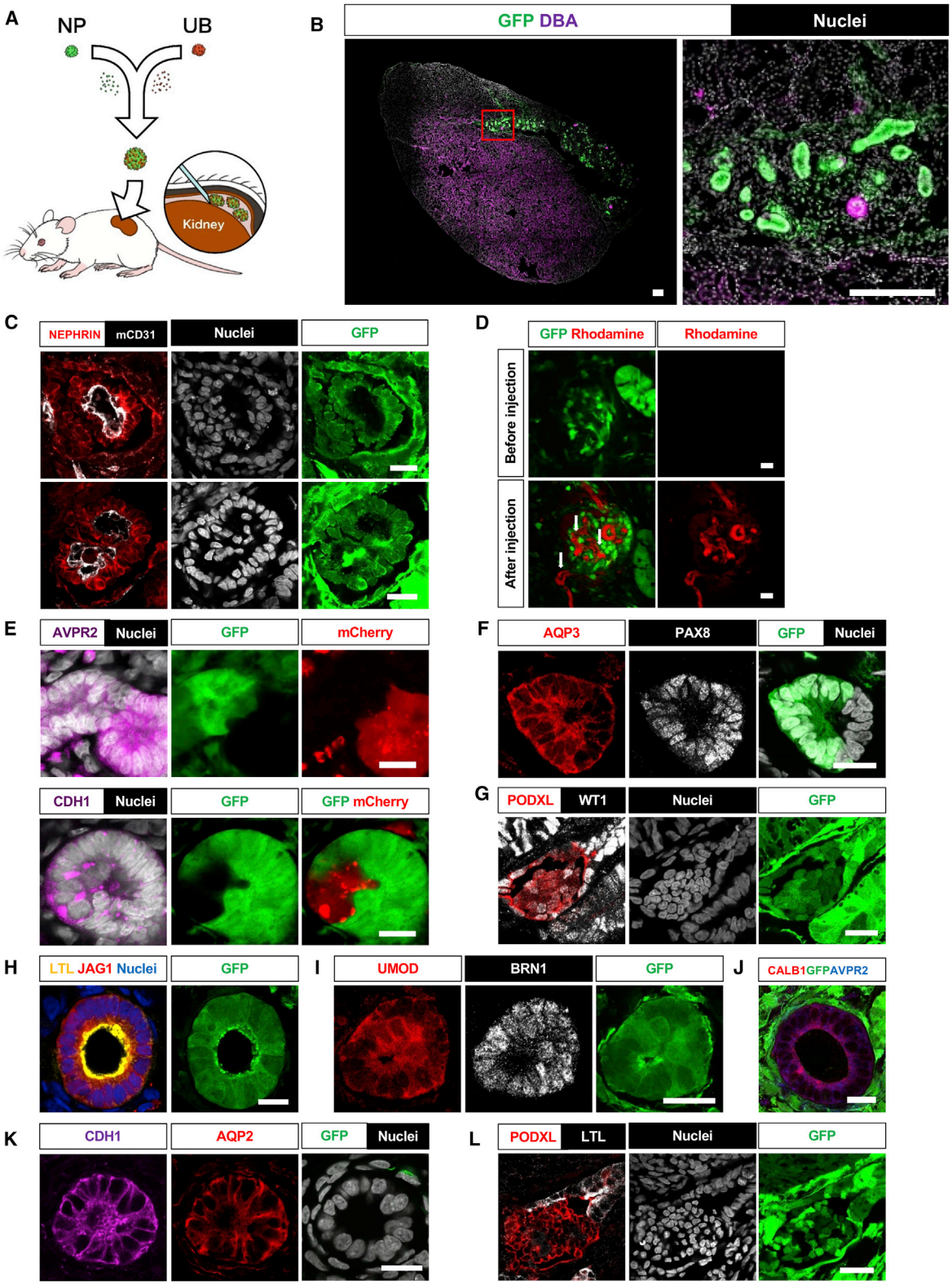

(legend on next page)

reported (Figures 4A, S7E, and S7F; Bantounas et al., 2018; Sharmin et al., 2016). As expected, the resultant kidney organoids 20 days after transplantation were vascularized by host ECs, as evidenced by positive anti-mouse CD31 staining, and the ECs integrated into human glomerulus-like structures with parietal epithelia of Bowman's capsule in the organoids (Figures 4B, 4C, and S7G). To address whether the vascularized network was functional, we observed the transplanted kidney organoids 10 days after transplantation by intravital imaging using multiphoton microscopy. After tail vein injections of rhodamine B-conjugated dextran, we identified vessel lumens penetrating into the hiPSC-derived glomerulus-like structures (Figures 4D, white arrows, and S7H; Video S1). We then examined epithelial connections in the organoids generated from 317-12-derived GFP$^+$ NPs and 511-3E-derived mCherry$^+$ UB cells and confirmed connections between GFP$^+$ tubular structures and mCherry$^+$ ductal structures, which were counterstained with anti-AVPR2 and anti-CDH1 antibodies (Figure 4E). We also found that the epithelial connecting points were positive for a marker of distal tubules or collecting ducts, AQP3, in organoids generated from 317-12-derived GFP$^+$ NPs and 1231A3-derived UB cells (Figure 4F). The organoids also contained GFP$^+$PODXL$^+$WT1$^+$ glomerulus (Figure 4G), GFP$^+$LTL$^+$JAGGED1$^+$ proximal tubule (Figures 4Hand S7I), GFP$^+$ UMOD$^+$BRN1$^+$ Henle's loop (Figure 4I), and GFP$^-$CALB1$^+$AVPR2$^+$ (Figure 4J) and GFP$^-$CDH1$^+$AQP2$^+$ collecting duct structures (Figure 4K) and showed the interconnection of Bowman's space and the luminal space of proximal tubules (Figure 4L). These results suggest that hiPSC-derived single NPs and UB cells developed vascularized kidney structures with interconnections between the renal tubules and collecting ducts *in vivo*.

DISCUSSION

Although previous studies induced CDX2$^+$ late PS cells toward NPs by treatment with CHIR99021 (Morizane et al., 2015; Taguchi et al., 2014; Takasato et al., 2015), the high concentration used may cause adverse effects, including cytotoxicity and unstable cell differentiation (Naujok et al., 2014). We instead succeeded in robustly and stably generating CDX2$^+$ late PS cells by adding Smad2/3 inhibitors after the PS induction stage without a high dose of GSK3 inhibitors. Recently, Loh et al. (2016) reported methods to induce mesoderm lineages, except for IM from hPSCs. In the present study, we succeeded in establishing an equally efficient method to induce LPM and PAM cells. Moreover, we could generate multiple IM-lineage cells in our systematic differentiation map.

The separate induction of metanephric and mesonephric NPs and UB cells in *in vitro* monolayer culture systems has not been fully investigated. RNA-seq analyses in this study showed that Act(+)-NPs strongly expressed HOXD11, whereas Act(−)-NPs did not upregulate posterior HOX cluster genes. In addition, a higher expression of ITGA8 was found in Act(−)-NPs compared with Act(+)-NPs, which may correlate with the higher Itga8 expression reported in mesonephric NPs compared with metanephric NPs in mouse embryos (Figure S2K; Müller et al., 1997). The analyses also showed that ROBO2 and FAT4 expression is significantly higher in Act(+)-NPs than in Act(−)-NPs (Table S2). It was reported that higher ROBO2 expression in MM negatively regulates the number of UB outgrowths from the nephric duct (Grieshammer et al., 2004; Wainwright et al., 2015) and that the number of outgrowths from the nephric duct in mesonephros is larger than in metanephros (Clapp, 2017). Another recent study reported that Fat4 mutant mice have ectopic UB formation and identified Fat4 as a regulator of ureteric budding and excessive RET signaling (Zhang et al., 2019). Therefore, our data are consistent with previous findings and indicate that a higher expression of ROBO2 and FAT4 in metanephric NPs than in mesonephric NPs leads to less outgrowth from the nephric duct in metanephros than in mesonephros.

In addition, the expression of two Henle's loop markers, *NKCC2* and *UMOD*, was higher in organoids derived from Act(+)-NPs than from Act(−)-NPs, which is consistent with the finding that mammalian mesonephros lacks Henle's loop (Wintour et al., 1996). However, another study reported that marker genes for early Henle's loop are expressed in mouse mesonephros (Georgas et al., 2011). Our RNA-seq analysis showed that the expression of mesonephric nephron markers (*TCN2*, *FBP1*, *SLC27A2*, and *ENTPD5*) and of early Henle's loop (*AADAC* and *GPD1*) was significantly upregulated in Act(−)-organoids compared with Act(−)-NPs, which is consistent with

Figure 4. *In Vivo* Reconstruction of Vascularized Kidney Structures from Induced Metanephric NPs and UB Cells

(A) Schematic showing the *in vivo* reconstruction of kidney structures.

(B) A lower magnification image of DBA staining of the human kidney graft generated from GFP$^+$ NPs and GFP$^-$ UB cells and host mouse kidney 20 days after transplantation. The right panel is a magnified image of the boxed area. Note that DBA$^+$ cells were found in the collecting ducts of the host mouse kidney and human kidney graft and that weak signals were also found in the distal tubules.

(C) Immunofluorescence analyses of NEPHRIN and mouse CD31 in glomerulus-like structures in the human kidney grafts 20 days after transplantation.

(D) Intra-vital 2-photon laser-scanning microscopic images of the human kidney graft from GFP$^+$ NPs and UB cells differentiated from hiPSCs constitutively expressing mCherry (mCherry$^+$ UB cells) before and after rhodamine B-conjugated dextran injection. The white arrows indicate vessel lumens penetrating into an hiPSC-derived glomerulus-like structure, as evidenced by rhodamine B fluorescence. Note that no mCherry$^+$ cells were observed in the areas before the dextran injection.

(E) Immunofluorescence analyses of markers for distal tubules or collecting ducts (AVPR2 and CDH1) show GFP$^+$ NP-derived distal tubules connected to mCherry$^+$ UB cell-derived collecting ducts.

(F) Immunofluorescence analyses of a distal tubule or collecting duct marker (AQP3) and PAX8 show GFP$^+$ NP-derived distal tubules connected to GFP$^-$ UB cell-derived collecting ducts.

(G–L) Immunofluorescence analyses of the kidney grafts generated from GFP$^+$ NPs and GFP$^-$ UB cells show GFP$^+$PODXL$^+$WT1$^+$ glomerulus (G), GFP$^+$LTL$^+$JAGGED1$^+$ proximal tubule (H), GFP$^+$UMOD$^+$BRN1$^+$ Henle's loop (I), GFP$^-$CALB1$^+$AVPR2$^+$ (J), and GFP$^-$CDH1$^+$AQP2$^+$ collecting ducts (K), and GFP$^+$PODXL$^+$ glomerulus and GFP$^+$LTL$^+$ proximal tubule (L). Note that Bowman's space is interconnected with the luminal space of the proximal tubule in (L). Scale bars, 200 μm in (B) and 20 μm in (C)–(L).

Georgas et al. (2011). Since confirming the similarity of our Act(−)-NPs with mesonephric NPs in human embryos is difficult due to limited embryo samples, we called our Act(−)-NPs mesonephric NP-like cells. Taken together with previous findings, our data indicate that mesonephric nephron contains cells that express markers for early Henle's loop, but not late or mature Henle's loop. Future studies should further characterize our Act(−)-NPs by comparing them to their counterparts in human embryos. Nonetheless, we established a differentiation system that can separately induce metanephric NPs and mesonephric NP-like cells as well as UB cells from hiPSCs, which should contribute to disclosing the developmental mechanisms of human kidneys.

Harari-Steinberg et al. (2013) identified committed NPs from human fetal kidney by culturing in serum-free defined conditions and prospective isolation by using NCAM1. The NP population showed clonogenic capacity, *in vivo* nephrogenic capability when grafted on the chick embryos, and therapeutic benefits in a mouse model of chronic progressive renal injury that mimics chronic kidney disease (CKD) in humans. Although NCAM1$^+$ populations contain both SIX2$^+$ and SIX2$^-$ progenitors in human fetal kidney, the group later showed that the NCAM1$^+$CD133$^-$ fraction more efficiently concentrates SIX2$^+$ NPs (Pode-Shakked et al., 2016). Furthermore, they dissected NCAM1$^+$CD133$^-$ progenitors according to epithelial cell adhesion molecule (EpCAM) expression by culturing in a defined medium modified from a previously reported NP expansion medium (Brown et al., 2015) and showed that the NCAM1$^+$CD133$^-$EpCAM$^-$ fraction contains a cap mesenchyme population that overexpresses SIX2, WT1, OSR1, CITED1, EYA1, SIX1, and CDH11 (Pode-Shakked et al., 2017). The hiPSC-derived metanephric NPs that we generated are close to that population in terms of the expression of the aforementioned markers evaluated by RNA-seq (data not shown) and nephrogenic potential *in vitro* and *in vivo*. Further comparisons of hiPSC-derived NPs with NCAM1$^+$CD133$^-$EpCAM$^-$ cells in the human fetal kidney, including functional comparisons, would contribute to the stable generation of genuine NPs from hiPSCs.

The present study also shows reciprocal interactions between NPs and UB cells in nephrogenic niches and the generation of human kidney organoids that contain collecting ducts that express multiple collecting duct lineage markers (CALB1, AQP2, AQP3, AQP4, AVPR2, PENDRIN, and ATP6V1B1), in addition to glomeruli and renal tubules. Moreover, our reconstructed kidney organoids showed nephron-constituting segments, including glomeruli, proximal and distal tubules, and Henle's loop, which contiguously connected to the collecting duct structures that differentiated from hiPSCs. Therefore, our differentiation system could contribute to understanding the mechanisms of the reciprocal interactions and interconnections between NP-derived tubules and UB-derived collecting ducts in humans.

Finally, one report implanted hiPSC-derived NP aggregates into the renal subcapsules of immunodeficient mice to generate vascularized glomeruli-like structures *in vivo* (Sharmin et al., 2016). Other studies generated vascularized kidney organoids by implanting hPSC-derived kidney lineage aggregates containing simultaneously induced NP- and UB-lineage cells using a differentiation protocol similar to Takasato et al. (2015) into immunodeficient mice subcutaneously (Bantounas et al., 2018; van den Berg et al., 2018). In the present study, we successfully vascularized kidney organoids generated from separately induced hiPSC-derived NPs and UB cells *in vivo*, in which the nephron structures differentiated from hiPSC-derived metanephric NPs contiguously connect to collecting duct structures derived from hiPSC-derived UB cells in the organoids. Dekel et al. (2003) found that the transplantation of human and porcine metanephric kidney precursor tissues only at optimal developmental time points (7–8 weeks of human gestation or 3.5–4 weeks of pig gestation) into mice survive, grow, differentiate into nephrons with a robust formation of vascularized glomeruli and tubules, and form a functional kidney organ that produces dilute urine. They also demonstrated decreased immunogenicity of the transplants of early human and pig kidney precursors compared with adult kidney transplants. However, our hiPSC-derived kidney grafts developed less vascularized glomeruli and did not form cyst structures containing urine (Figure 4B). Future studies should examine the optimal differentiation stages of hiPSC-derived kidney progenitors for transplantation so that the resultant grafts frequently develop functional nephrons with vascularized glomeruli that are suitable for transplantation in humans with less immunogenicity compared with adult kidneys presently used in renal transplantation.

In summary, we established stepwise differentiation protocols for the three main kidney progenitor cells and LPM and PAM in a monolayer culture system. Our system reproduces multiple developmental steps with stage-specific gene expressions accurately. Moreover, it can generate vascularized interconnected kidney organoids from the induced progenitors. However, some limitations must be overcome. We did not achieve the extensive branching morphogenesis of UBs. Future studies should establish the induction protocol of renal stromal cells, because these cell types may contribute to the UB branching capacity (Taguchi and Nishinakamura, 2017). We should also improve glomerular, tubular, and ductal functional maturity. Nevertheless, the differentiation protocols and kidney reconstruction methods established in this study may contribute to understanding the mechanisms underlying human kidney development and congenital renal disorders as well as the mechanisms generating suitable transplantable cells for regenerative therapies.

STAR★METHODS

Detailed methods are provided in the online version of this paper and include the following:

- KEY RESOURCES TABLE
- LEAD CONTACT AND MATERIALS AVAILABILITY
- EXPERIMENTAL MODEL AND SUBJECT DETAILS
  - Human Tissues
  - Mice
  - hiPSC Line and Maintenance
- METHOD DETAILS
  - Differentiation Protocols
  - Immunostaining
  - Flow Cytometry and Cell Sorting
  - RT-PCR and Real-time Quantitative RT-PCR (qRT-PCR)

SUPPLEMENTAL INFORMATION

Supplemental Information can be found online at https://doi.org/10.1016/j.celrep.2020.03.040.

ACKNOWLEDGMENTS

The authors would like to thank (all from CiRA, Kyoto University) Drs. Knut Woltjen, Kanae Mitsunaga, Maki Kotaka, Katsutaro Yasuda, Naoko Katagiri, and Azuma Kimura, Mr. Shunsuke Kihara, Mr. Akito Tanaka, and Ms. Tomomi Sudo for their technical support and valuable scientific discussions; Dr. Peter Karagiannis for critically reading and revising the manuscript; Ms. Akiko Hasegawa and Ms. Midori Sakiyama for RNA sequencing; and Dr. Misaki Ouchida for the schematic illustration. They also thank Drs. Hiroshi Nagashima and Hitomi Matsunari, Meiji University, for providing resources, and Drs. Takashi Yokoo, Kei Matsumoto, and Toshinari Fujimoto, Jikei University School of Medicine, for technical advice on the transplantation experiments. This study was supported by the Japan Agency for Medical Research and Development (AMED) through its research grants "Projects for Technological Development, Core Center for iPS Cell Research, and the Acceleration Program for Intractable Diseases Research Utilizing Disease-Specific iPS Cells, Research Center Network for Realization of Regenerative Medicine" and "Practical Research Project for Rare/Intractable Diseases" to K.O., and the Japan Society for the Promotion of Science (JSPS) Grant-in-Aid for Young Scientists (B) 18K15121 to S. Sakamoto, Grants-in-Aid for Scientific Research (C) 15K06921 and 17KT0108 to A.W., and Grants-in-Aid for Scientific Research (B) 18H02826 to K.O. T.K. was supported by fellowship from the JSPS.

AUTHOR CONTRIBUTIONS

Conceptualization, H.T., T.K., S. Sueta, T.A., A.W., and K.O.; Methodology, H.T., T.K., and S. Sueta; Investigation, H.T., T.K., S. Sueta, T.A., S. Sakamoto, C.O., S.M., T.N., N.O., D.T., M.N., T.S., M.R., and Z.L.; Writing – Original Draft, H.T., T.K., and S. Sueta; Writing – Review & Editing, T.A., A.W., and K.O.; Funding Acquisition, T.K., S. Sakamoto, A.W., and K.O.; Resources, K.O.; Project Administration, H.T., T.K., S. Sueta, T.A., A.W., and K.O.; Supervision, M.S., M.I., A.W., and K.O.

DECLARATION OF INTERESTS

K.O. is a founder and member without salary of the scientific advisory boards of iPS Portal and a founder and the chief scientific advisor of RegeNephro. T.A. is a founder and scientific advisor of RegeNephro Co., Ltd. Differentiation method for nephron progenitor cells from hiPSCs (PCT/JP2018/019886, WO 2018/216743).

Received: March 26, 2018
Revised: January 17, 2020
Accepted: March 13, 2020
Published: April 7, 2020

REFERENCES

Ameku, T., Taura, D., Sone, M., Numata, T., Nakamura, M., Shiota, F., Toyoda, T., Matsui, S., Araoka, T., Yasuno, T., et al. (2016). Identification of MMP1 as a novel risk factor for intracranial aneurysms in ADPKD using iPSC models. Sci. Rep. *6*, 30013.

Bantounas, I., Ranjzad, P., Tengku, F., Silajdžić, E., Forster, D., Asselin, M.C., Lewis, P., Lennon, R., Plagge, A., Wang, Q., et al. (2018). Generation of Functioning Nephrons by Implanting Human Pluripotent Stem Cell-Derived Kidney Progenitors. Stem Cell Reports *10*, 766–779.

Brown, A.C., Muthukrishnan, S.D., and Oxburgh, L. (2015). A synthetic niche for nephron progenitor cells. Dev. Cell *34*, 229–241.

Cha, S.W., Hwang, Y.S., Chae, J.P., Lee, S.Y., Lee, H.S., Daar, I., Park, M.J., and Kim, J. (2004). Inhibition of FGF signaling causes expansion of the endoderm in Xenopus. Biochem. Biophys. Res. Commun. *315*, 100–106.

Chen, L., Lee, J.W., Chou, C.L., Nair, A.V., Battistone, M.A., Păunescu, T.G., Merkulova, M., Breton, S., Verlander, J.W., Wall, S.M., et al. (2017). Transcriptomes of major renal collecting duct cell types in mouse identified by single-cell RNA-seq. Proc. Natl. Acad. Sci. USA *114*, E9989–E9998.

Clapp, W.L. (2017). Renal Development and Anatomy. In Silva's Diagnostic Renal Pathology, Second Edition, X.J. Zhou, Z.G. Laszik, T. Nadasdy, and V.D. D'Agati, eds. (Cambridge University Press), pp. 1–56.

Costantini, F., and Kopan, R. (2010). Patterning a complex organ: branching morphogenesis and nephron segmentation in kidney development. Dev. Cell *18*, 698–712.

Dekel, B., Burakova, T., Arditti, F.D., Reich-Zeliger, S., Milstein, O., Aviel-Ronen, S., Rechavi, G., Friedman, N., Kaminski, N., Passwell, J.H., and Reisner, Y. (2003). Human and porcine early kidney precursors as a new source for transplantation. Nat. Med. *9*, 53–60.

Evans, A.L., Faial, T., Gilchrist, M.J., Down, T., Vallier, L., Pedersen, R.A., Wardle, F.C., and Smith, J.C. (2012). Genomic targets of Brachyury (T) in differentiating mouse embryonic stem cells. PLoS One *7*, e33346.

Faial, T., Bernardo, A.S., Mendjan, S., Diamanti, E., Ortmann, D., Gentsch, G.E., Mascetti, V.L., Trotter, M.W., Smith, J.C., and Pedersen, R.A. (2015). Brachyury and SMAD signalling collaboratively orchestrate distinct mesoderm and endoderm gene regulatory networks in differentiating human embryonic stem cells. Development *142*, 2121–2135.

Gaunt, S.J., George, M., and Paul, Y.L. (2013). Direct activation of a mouse Hoxd11 axial expression enhancer by Gdf11/Smad signalling. Dev. Biol. *383*, 52–60.

Georgas, K.M., Chiu, H.S., Lesieur, E., Rumballe, B.A., and Little, M.H. (2011). Expression of metanephric nephron-patterning genes in differentiating mesonephric tubules. Dev. Dyn. *240*, 1600–1612.

Grassmeyer, J., Mukherjee, M., deRiso, J., Hettinger, C., Bailey, M., Sinha, S., Visvader, J.E., Zhao, H., Fogarty, E., and Surendran, K. (2017). Elf5 is a principal cell lineage specific transcription factor in the kidney that contributes to Aqp2 and Avpr2 gene expression. Dev. Biol. *424*, 77–89.

Grieshammer, U., Le Ma, Plump, A.S., Wang, F., Tessier-Lavigne, M., and Martin, G.R. (2004). SLIT2-mediated ROBO2 signaling restricts kidney induction to a single site. Dev. Cell *6*, 709–717.

Harari-Steinberg, O., Metsuyanim, S., Omer, D., Gnatek, Y., Gershon, R., Pri-Chen, S., Ozdemir, D.D., Lerenthal, Y., Noiman, T., Ben-Hur, H., et al. (2013). Identification of human nephron progenitors capable of generation of kidney structures and functional repair of chronic renal disease. EMBO Mol. Med. *5*, 1556–1568.

Harding, S.D., Armit, C., Armstrong, J., Brennan, J., Cheng, Y., Haggarty, B., Houghton, D., Lloyd-MacGilp, S., Pi, X., Roochun, Y., et al. (2011). The GUDMAP database–an online resource for genitourinary research. Development *138*, 2845–2853.

Homma, K., Sone, M., Taura, D., Yamahara, K., Suzuki, Y., Takahashi, K., Sonoyama, T., Inuzuka, M., Fukunaga, Y., Tamura, N., et al. (2010). Sirt1 plays an important role in mediating greater functionality of human ES/iPS-derived vascular endothelial cells. Atherosclerosis *212*, 42–47.

Houle, M., Sylvestre, J.R., and Lohnes, D. (2003). Retinoic acid regulates a subset of Cdx1 function in vivo. Development *130*, 6555–6567.

Iyer, D., Gambardella, L., Bernard, W.G., Serrano, F., Mascetti, V.L., Pedersen, R.A., Sinha, S., and Talasila, A. (2016). Robust derivation of epicardium and its differentiated smooth muscle cell progeny from human pluripotent stem cells. Development *143*, 904.

James, D., Nam, H.S., Seandel, M., Nolan, D., Janovitz, T., Tomishima, M., Studer, L., Lee, G., Lyden, D., Benezra, R., et al. (2010). Expansion and maintenance of human embryonic stem cell-derived endothelial cells by TGFbeta inhibition is Id1 dependent. Nat. Biotechnol. *28*, 161–166.

Keenan, I.D., Sharrard, R.M., and Isaacs, H.V. (2006). FGF signal transduction and the regulation of Cdx gene expression. Dev. Biol. *299*, 478–488.

Kovacic, J.C., Mercader, N., Torres, M., Boehm, M., and Fuster, V. (2012). Epithelial-to-mesenchymal and endothelial-to-mesenchymal transition: from cardiovascular development to disease. Circulation *125*, 1795–1808.

Lefevre, J.G., Chiu, H.S., Combes, A.N., Vanslambrouck, J.M., Ju, A., Hamilton, N.A., and Little, M.H. (2017). Self-organisation after embryonic kidney dissociation is driven via selective adhesion of ureteric epithelial cells. Development *144*, 1087–1096.

Lengerke, C., Schmitt, S., Bowman, T.V., Jang, I.H., Maouche-Chretien, L., McKinney-Freeman, S., Davidson, A.J., Hammerschmidt, M., Rentzsch, F., Green, J.B., et al. (2008). BMP and Wnt specify hematopoietic fate by activation of the Cdx-Hox pathway. Cell Stem Cell *2*, 72–82.

Li, Z., Araoka, T., Wu, J., Liao, H.K., Li, M., Lazo, M., Zhou, B., Sui, Y., Wu, M.Z., Tamura, I., et al. (2016). 3D Culture Supports Long-Term Expansion of Mouse and Human Nephrogenic Progenitors. Cell Stem Cell *19*, 516–529.

Lindström, N.O., McMahon, J.A., Guo, J., Tran, T., Guo, Q., Rutledge, E., Parvez, R.K., Saribekyan, G., Schuler, R.E., Liao, C., et al. (2018a). Conserved and Divergent Features of Human and Mouse Kidney Organogenesis. J. Am. Soc. Nephrol. *29*, 785–805.

Lindström, N.O., Guo, J., Kim, A.D., Tran, T., Guo, Q., De Sena Brandine, G., Ransick, A., Parvez, R.K., Thornton, M.E., Baskin, L., et al. (2018b). Conserved and Divergent Features of Mesenchymal Progenitor Cell Types within the Cortical Nephrogenic Niche of the Human and Mouse Kidney. J. Am. Soc. Nephrol. *29*, 806–824.

Lindström, N.O., Tran, T., Guo, J., Rutledge, E., Parvez, R.K., Thornton, M.E., Grubbs, B., McMahon, J.A., and McMahon, A.P. (2018c). Conserved and Divergent Molecular and Anatomic Features of Human and Mouse Nephron Patterning. J. Am. Soc. Nephrol. *29*, 825–840.

Loh, K.M., Chen, A., Koh, P.W., Deng, T.Z., Sinha, R., Tsai, J.M., Barkal, A.A., Shen, K.Y., Jain, R., Morganti, R.M., et al. (2016). Mapping the Pairwise Choices Leading from Pluripotency to Human Bone, Heart, and Other Mesoderm Cell Types. Cell *166*, 451–467.

Lu, B.C., Cebrian, C., Chi, X., Kuure, S., Kuo, R., Bates, C.M., Arber, S., Hassell, J., MacNeil, L., Hoshi, M., et al. (2009). Etv4 and Etv5 are required downstream of GDNF and Ret for kidney branching morphogenesis. Nat. Genet. *41*, 1295–1302.

Mae, S.I., Shono, A., Shiota, F., Yasuno, T., Kajiwara, M., Gotoda-Nishimura, N., Arai, S., Sato-Otubo, A., Toyoda, T., Takahashi, K., et al. (2013). Monitoring and robust induction of nephrogenic intermediate mesoderm from human pluripotent stem cells. Nat. Commun. *4*, 1367.

Mae, S.I., Ryosaka, M., Toyoda, T., Matsuse, K., Oshima, Y., Tsujimoto, H., Okumura, S., Shibasaki, A., and Osafune, K. (2018). Generation of branching ureteric bud tissues from human pluripotent stem cells. Biochem. Biophys. Res. Commun. *495*, 954–961.

Mendjan, S., Mascetti, V.L., Ortmann, D., Ortiz, M., Karjosukarso, D.W., Ng, Y., Moreau, T., and Pedersen, R.A. (2014). NANOG and CDX2 pattern distinct subtypes of human mesoderm during exit from pluripotency. Cell Stem Cell *15*, 310–325.

Meyer, B.I., and Gruss, P. (1993). Mouse Cdx-1 expression during gastrulation. Development *117*, 191–203.

Morizane, R., Lam, A.Q., Freedman, B.S., Kishi, S., Valerius, M.T., and Bonventre, J.V. (2015). Nephron organoids derived from human pluripotent stem cells model kidney development and injury. Nat. Biotechnol. *33*, 1193–1200.

Mugford, J.W., Sipilä, P., Kobayashi, A., Behringer, R.R., and McMahon, A.P. (2008). Hoxd11 specifies a program of metanephric kidney development within the intermediate mesoderm of the mouse embryo. Dev. Biol. *319*, 396–405.

Müller, U., Wang, D., Denda, S., Meneses, J.J., Pedersen, R.A., and Reichardt, L.F. (1997). Integrin $\alpha 8\beta 1$ is critically important for epithelial-mesenchymal interactions during kidney morphogenesis. Cell *88*, 603–613.

Nakajima, T., Shibata, M., Nishio, M., Nagata, S., Alev, C., Sakurai, H., Toguchida, J., and Ikeya, M. (2018). Modeling human somite development and fibrodysplasia ossificans progressiva with induced pluripotent stem cells. Development *145*, dev165431.

Naujok, O., Lentes, J., Diekmann, U., Davenport, C., and Lenzen, S. (2014). Cytotoxicity and activation of the Wnt/beta-catenin pathway in mouse embryonic stem cells treated with four GSK3 inhibitors. BMC Res. Notes *7*, 273.

Nguyen, M.T.X., Okina, E., Chai, X., Tan, K.H., Hovatta, O., Ghosh, S., and Tryggvason, K. (2016). Differentiation of Human Embryonic Stem Cells to Endothelial Progenitor Cells on Laminins in Defined and Xeno-free Systems. Stem Cell Reports *7*, 802–816.

Oceguera-Yanez, F., Kim, S.I., Matsumoto, T., Tan, G.W., Xiang, L., Hatani, T., Kondo, T., Ikeya, M., Yoshida, Y., Inoue, H., and Woltjen, K. (2016). Engineering the AAVS1 locus for consistent and scalable transgene expression in human iPSCs and their differentiated derivatives. Methods *101*, 43–55.

Oh, S.P., Yeo, C.Y., Lee, Y., Schrewe, H., Whitman, M., and Li, E. (2002). Activin type IIA and IIB receptors mediate Gdf11 signaling in axial vertebral patterning. Genes Dev. *16*, 2749–2754.

Okita, K., Yamakawa, T., Matsumura, Y., Sato, Y., Amano, N., Watanabe, A., Goshima, N., and Yamanaka, S. (2013). An efficient nonviral method to generate integration-free human-induced pluripotent stem cells from cord blood and peripheral blood cells. Stem Cells *31*, 458–466.

Pode-Shakked, N., Pleniceanu, O., Gershon, R., Shukrun, R., Kanter, I., Bucris, E., Pode-Shakked, B., Tam, G., Tam, H., Caspi, R., et al. (2016). Dissecting stages of human kidney development and tumorigenesis with surface markers affords simple prospective purification of nephron stem cells. Sci. Rep. *6*, 23562.

Pode-Shakked, N., Gershon, R., Tam, G., Omer, D., Gnatek, Y., Kanter, I., Oriel, S., Katz, G., Harari-Steinberg, O., Kalisky, T., and Dekel, B. (2017). Evidence of in vitro perservation of human nephrogenesis at the single-cell level. Stem Cell Reports *9*, 279–291.

Przepiorski, A., Sander, V., Tran, T., Hollywood, J.A., Sorrenson, B., Shih, J.H., Wolvetang, E.J., McMahon, A.P., Holm, T.M., and Davidson, A.J. (2018). A Simple Bioreactor-Based Method to Generate Kidney Organoids from Pluripotent Stem Cells. Stem Cell Reports *11*, 470–484.

Roost, M.S., van Iperen, L., Ariyurek, Y., Buermans, H.P., Arindrarto, W., Devalla, H.D., Passier, R., Mummery, C.L., Carlotti, F., de Koning, E.J., et al. (2015). KeyGenes, a Tool to Probe Tissue Differentiation Using a Human Fetal Transcriptional Atlas. Stem Cell Reports *4*, 1112–1124.

Sakaki-Yumoto, M., Liu, J., Ramalho-Santos, M., Yoshida, N., and Derynck, R. (2013). Smad2 is essential for maintenance of the human and mouse primed pluripotent stem cell state. J. Biol. Chem. *288*, 18546–18560.

Schneider, C.A., Rasband, W.S., and Eliceiri, K.W. (2012). NIH Image to ImageJ: 25 years of image analysis. Nat. Methods *9*, 671–675.

Sharmin, S., Taguchi, A., Kaku, Y., Yoshimura, Y., Ohmori, T., Sakuma, T., Mukoyama, M., Yamamoto, T., Kurihara, H., and Nishinakamura, R. (2016). Human Induced Pluripotent Stem Cell-Derived Podocytes Mature into Vascularized Glomeruli upon Experimental Transplantation. J. Am. Soc. Nephrol. *27*, 1778–1791.

Streit, A., Lee, K.J., Woo, I., Roberts, C., Jessell, T.M., and Stern, C.D. (1998). Chordin regulates primitive streak development and the stability of induced neural cells, but is not sufficient for neural induction in the chick embryo. Development *125*, 507–519.

Taguchi, A., and Nishinakamura, R. (2017). Higher-Order Kidney Organogenesis from Pluripotent Stem Cells. Cell Stem Cell *21*, 730–746.e6.

Taguchi, A., Kaku, Y., Ohmori, T., Sharmin, S., Ogawa, M., Sasaki, H., and Nishinakamura, R. (2014). Redefining the in vivo origin of metanephric nephron progenitors enables generation of complex kidney structures from pluripotent stem cells. Cell Stem Cell *14*, 53–67.

Takasato, M., Er, P.X., Becroft, M., Vanslambrouck, J.M., Stanley, E.G., Elefanty, A.G., and Little, M.H. (2014). Directing human embryonic stem cell differentiation towards a renal lineage generates a self-organizing kidney. Nat. Cell Biol. *16*, 118–126.

Takasato, M., Er, P.X., Chiu, H.S., Maier, B., Baillie, G.J., Ferguson, C., Parton, R.G., Wolvetang, E.J., Roost, M.S., Chuva de Sousa Lopes, S.M., and Little, M.H. (2015). Kidney organoids from human iPS cells contain multiple lineages and model human nephrogenesis. Nature *526*, 564–568.

Takebe, T., Zhang, R.R., Koike, H., Kimura, M., Yoshizawa, E., Enomura, M., Koike, N., Sekine, K., and Taniguchi, H. (2014). Generation of a vascularized and functional human liver from an iPSC-derived organ bud transplant. Nat. Protoc. *9*, 396–409.

Toyohara, T., Mae, S., Sueta, S., Inoue, T., Yamagishi, Y., Kawamoto, T., Kasahara, T., Hoshina, A., Toyoda, T., Tanaka, H., et al. (2015). Cell Therapy Using Human Induced Pluripotent Stem Cell-Derived Renal Progenitors Ameliorates Acute Kidney Injury in Mice. Stem Cells Transl. Med. *4*, 980–992.

van den Berg, C.W., Ritsma, L., Avramut, M.C., Wiersma, L.E., van den Berg, B.M., Leuning, D.G., Lievers, E., Koning, M., Vanslambrouck, J.M., Koster, A.J., et al. (2018). Renal Subcapsular Transplantation of PSC-Derived Kidney Organoids Induces Neo-vasculogenesis and Significant Glomerular and Tubular Maturation In Vivo. Stem Cell Reports *10*, 751–765.

Wainwright, E.N., Wilhelm, D., Combes, A.N., Little, M.H., and Koopman, P. (2015). ROBO2 restricts the nephrogenic field and regulates Wolffian duct-nephrogenic cord separation. Dev. Biol. *404*, 88–102.

Wang, P., Chen, Y., Yong, J., Cui, Y., Wang, R., Wen, L., Qiao, J., and Tang, F. (2018). Dissecting the Global Dynamic Molecular Profiles of Human Fetal Kidney Development by Single-Cell RNA Sequencing. Cell Rep. *24*, 3554–3567.e3.

Wintour, E.M., Alcorn, D., Butkus, A., Congiu, M., Earnest, L., Pompolo, S., and Potocnik, S.J. (1996). Ontogeny of hormonal and excretory function of the meso- and metanephros in the ovine fetus. Kidney Int. *50*, 1624–1633.

Xia, Y., Nivet, E., Sancho-Martinez, I., Gallegos, T., Suzuki, K., Okamura, D., Wu, M.Z., Dubova, I., Esteban, C.R., Montserrat, N., et al. (2013). Directed differentiation of human pluripotent cells to ureteric bud kidney progenitor-like cells. Nat. Cell Biol. *15*, 1507–1515.

Zhang, H., Bagherie-Lachidan, M., Badouel, C., Enderle, L., Peidis, P., Bremner, R., Kuure, S., Jain, S., and McNeill, H. (2019). FAT4 Fine-Tunes Kidney Development by Regulating RET Signaling. Dev. Cell *48*, 780–792.e4.

Zhong, T.P., Childs, S., Leu, J.P., and Fishman, M.C. (2001). Gridlock signalling pathway fashions the first embryonic artery. Nature *414*, 216–220.

STAR★METHODS

KEY RESOURCES TABLE

REAGENT or RESOURCE	SOURCE	IDENTIFIER
Antibodies		
AQP2	Santa Cruz	CAT.# sc-9880; RRID:AB_10988758
AQP2	Abcam	CAT.# ab62628-100; RRID:AB_2227510
AQP3	Santa Cruz	CAT.# sc-518001
AQP4	Santa Cruz	CAT.# sc-32739; RRID:AB_626695
ATP6V1B1	Abcam	CAT. # ab192612; RRID:AB_2810993
AVPR2	Sigma-Aldrich	CAT.# HPA046678; RRID:AB_2679747
BRACHYURY	R&D	CAT. # AF2085; RRID:AB_2200235
BRN1 (POU3F3)	Novus Biologicals	CAT. # NBP2-57011
CALB1	Sigma-Aldrich	CAT. # c9848; RRID:AB_476894
CALB1	Synaptic Systems	CAT. # 214004; RRID:AB_10550535
CDH1	BD	CAT. # 610181; RRID:AB_397580
CDH6	R&D	CAT. # MAB2715; RRID:AB_907139
CDX1	Novus Biologicals	CAT. # NBP1-49538; RRID:AB_10011593
CDX2	Abcam	CAT. # Ab157524; RRID:AB_2721036
CD31/PCAM1	eBioscience	CAT. # 14-0319-80; RRID:AB_467203
CD31(mouse)	Dianova	CAT. # DIA-310; RRID:AB_2631039
CK8	Abcam	CAT. # ab9023; RRID:AB_306948
CK19	Abcam	CAT. # ab52625; RRID:AB_2281020
DBA	Vector laboratories	CAT. # B-1035; RRID:AB_2314288
eNOS	BD	CAT. # 610296; RRID:AB_397690
GATA3	Cell signaling	CAT. # 5852S; RRID:AB_10835690
GATA3	R&D	CAT. # AF2605; RRID:AB_2108571
GFP	Nacalai tesque	CAT. # 04404-84; RRID:AB_10013361
HNF1B	Sigma-Aldrich	CAT. # HPA002083; RRID:AB_1080232
HOXD11	Abcam	CAT. # ab55255; RRID:AB_942003
ITGA8	R&D	CAT. # AF4076; RRID:AB_2296280
JAGGED1	Santa Cruz	CAT. # sc-6011; RRID:AB_649689
LEF1	R&D	CAT. # AF7647
LHX1	R&D	CAT. # MAB2725; RRID:AB_2135636
LTL	Vector laboratories	CAT. # B-1325; RRID:AB_2336558
mCherry	Takara Bio	CAT. # 632496; RRID:AB_10013483
mCherry	MBL	CAT. # M208-3
NEPHRIN	PROGEN	CAT. # GP-N2; RRID:AB_1542487
NKCC2	Thermo Fisher Scientific	CAT. # PA5-41995; RRID:AB_2607911
OCT4	R&D	CAT. # AF2085; RRID:AB_2200235
PAX2	Biolegend	CAT. # 901001; RRID:AB_2565001
PAX2	Covance	CAT. # PRB-276P; RRID:AB_291611
PAX3	DSHB	CAT. # Clone:C2; RRID:AB_528426
PAX8	Proteintech	CAT. # 10336-1-AP; RRID:AB_2236705
PENDRIN	MBL	CAT. # K0143-3; RRID:AB_592717
PENDRIN	Bioss	CAT. # bs-6787R; RRID:AB_11058651
PODOCALYXIN	R&D	CAT. # AF1658; RRID:AB_354920
RET	R&D	CAT. # AF1485; RRID:AB_354820

(*Continued on next page*)

Continued

REAGENT or RESOURCE	SOURCE	IDENTIFIER
SALL1	PERSEUS PROTEOMICS	CAT. # PP-K9814-00; RRID:AB_2183228
SIX1	Cell signaling	CAT. # 12891S; RRID:AB_2753209
SIX2	Proteintech	CAT. # 11562-1-AP; RRID:AB_2189084
SOX9	R&D	CAT. # AF3075; RRID:AB_2194160
TBX6	R&D	CAT. # AF4744; RRID:AB_2200834
UMOD (THP)	Novus Biologicals	CAT. # NBP1-50321; RRID:AB_10012519
WT1	Santa Cruz	CAT. # sc-192; RRID:AB_632611
WT1	Santa Cruz	CAT. # SC-393498
WT1	Abcam	CAT. # ab89901; RRID:AB_2043201
Alexa Fluor 488 Donkey Anti-mouse IgG (H+L)	Thermo Fisher Scientific	CAT. # A21202; RRID:AB_141607
Alexa Fluor 546 Donkey Anti-mouse IgG (H+L)	Thermo Fisher Scientific	CAT. # A10036; RRID:AB_2534012
Alexa Fluor 647 Donkey Anti-mouse IgG (H+L)	Thermo Fisher Scientific	CAT. # A31571; RRID:AB_162542
Alexa Fluor 488 Donkey Anti-Rabbit IgG (H+L)	Thermo Fisher Scientific	CAT. # A21206; RRID:AB_2535792
Alexa Fluor 546 Donkey Anti-Rabbit IgG (H+L)	Thermo Fisher Scientific	CAT. # A10040; RRID:AB_2534016
Alexa Fluor 647 Donkey Anti-Rabbit IgG (H+L)	Thermo Fisher Scientific	CAT. # A31573; RRID:AB_2536183
Alexa Fluor 488 Donkey Anti-Goat IgG (H+L)	Thermo Fisher Scientific	CAT. # A11055; RRID:AB_2534102
Alexa Fluor 546 Donkey Anti-Goat IgG (H+L)	Thermo Fisher Scientific	CAT. # A11056; RRID:AB_142628
Alexa Fluor 647 Donkey Anti-Goat IgG (H+L)	Thermo Fisher Scientific	CAT. # A21447; RRID:AB_141844
Alexa Fluor 488 Donkey Anti-rat IgG (H+L)	Thermo Fisher Scientific	CAT. # A21208; RRID:AB_141709
Streptavidin, Alexa Fluor 488 conjugate	Thermo Fisher Scientific	CAT. # S32354; RRID:AB_2315383
Streptavidin, Alexa Fluor 546 conjugate	Thermo Fisher Scientific	CAT. # S11225; RRID:AB_2532130
Streptavidin, Alexa Fluor 647 conjugate	Thermo Fisher Scientific	CAT. # S32357
Streptavidin, DyLight 405 conjugate	Thermo Fisher Scientific	CAT. # 21831
Alexa Fluor 647 Donkey Anti-Rat IgG (H+L)	Jackson ImmunoResearch Inc.	CAT. # 712-605-150; RRID:AB_2340693
Donkey Anti-Guinea Pig IgG labeled with Cyanine Cy3	Jackson ImmunoResearch Inc.	CAT. # 706-165-148; RRID:AB_2340460
Alexa Fluor 488 Donkey Anti-Guinea Pig IgG (H+L)	Jackson ImmunoResearch Inc.	CAT. # 706-545-148
Alexa Fluor 647 Donkey Anti-Guinea Pig IgG (H+L)	Jackson ImmunoResearch Inc.	CAT. # 706-605-148; RRID:AB_2340476
CFTM 405S Donkey Anti-Goat IgG (H+L)	Biotium	CAT. # 20416
Biological Samples		
Human Fetal Kidney QUICK-Clone cDNA	TaKaRa Bio	CAT. # 637229
Normal Frozen Tissue: Kidney (age 28 weeks)	US Biomax Inc.	CAT. # HuFFN020
Frozen Tissue Section: Kidney (age 78 years old)	BioChain	CAT. # T1234142
Chemicals, Peptides, and Recombinant Proteins		
Accutase	Innovative Cell Technologies	CAT. # AT104
Accumax	Innovative Cell Technologies	CAT. # AM105
A-83-01	Wako	CAT. # 035-24113
B-27 Supplement minus vitamin A	Thermo Fisher Scientific	CAT. # 12587001
BMP-4	PeproTech	CAT. # AF-120-05ET
BMP-7	R&D	CAT. # 354-BP
Collagenase type IV	Thermo Fisher Scientific	CAT. # 17104019
CHIR99021	Axon	CAT. # AXN-AXON1386-25
DAPT	R&D	CAT. # 2634/10
DMEM/F-12, GlutaMAX	Thermo Fisher Scientific	CAT. # 10565042
Essential 6 Medium	Thermo Fisher Scientific	CAT. # A1516401
Human FGF basic	WAKO	CAT. # 060-04543
Human FGF acidic	R&D	CAT. # 231-BC-025
Human FGF 8	Peprotech	CAT. # 100-25
Human FGF 9	Peprotech	CAT. # 100-23
Human GDNF	R&D	CAT. # 212-GD-010

(*Continued on next page*)

Continued

REAGENT or RESOURCE	SOURCE	IDENTIFIER
iMatrix-511 silk	Nippi	CAT. # 892021
KnockOut Serum Replacement	Thermo Fisher Scientific	CAT. # A3181502
Laminin 411	Biolamina	CAT. # BLA-LN411-02
LDN193189	Wako	CAT. # 124-06011
Matrigel	BD	CAT. # 354230
NOGGIN	Peprotech	CAT. # 120-10C
Penicillin-Streptomycin	Thermo Fisher Scientific	CAT. # 15140122
Primate ES Cell Medium	ReproCELL	CAT. # RCHEMD001
Primate Repro FF2 medium	ReproCELL	CAT. # RCHEMD006
IWR-1	Sigma-Aldrich	CAT. # 10161
Retinoic Acid	Sigma-Aldrich	CAT. # R2625
StemPro-34 SFM	StemPro-34 SFM	CAT. # 10639-011
TTNPB	Santa Cruz	CAT. # sc-203303
Trypsin-EDTA (0.25%)	Thermo Fisher Scientific	CAT. # 25200072
Thiazovivin	Santa Cruz	CAT. # sc-361380
Y27632	Wako	CAT. # 034-24024
Seprafilm	Kakenseiyaku	CAT. # 4987-042-36001-8
Stem Fit AK02N	Takara Bio	CAT. # AK02N
VEGF	Peprotech	CAT. # 100-20
Critical Commercial Assays		
KAPA Stranded mRNA-Seq Kit	KAPA Biosystems	CAT. # KK8400
miRNeasy Mini Kit	QIAGEN	CAT. # 217004
RNeasy Mini kit	QIAGEN	CAT. # 74106
ReverTra Ace	TOYOBO	CAT. # TRT-101
Superscript III reverse transcriptase	Thermo Fisher Scientific	CAT. # 18080093
SureCell WTA 3′Library Prep Kit	illumina	CAT. # 20014280
SYBR Premix Ex TaqII	TaKaRa Bio	CAT. # RR820B
TaKaRa Ex-Taq	TaKaRa Bio	CAT. # RR001B
Thunderbird SYBR qPCR Mix	TOYOBO	CAT. # QPS-201
Deposited Data		
RNA sequencing data	This paper	GEO: GSE146119
Human reference genome hg19	UCSC	http://hgdownload.soe.ucsc.edu/downloads.html#human
A human fetal transcriptional atlas	Roost et al., 2015	GEO: GSE66302
RNA sequencing data of kidney organoids	Takasato et al., 2015	GEO: GSE70101
Single Cell RNA-Seq profiling human embryonic kidney cortex cells	Lindström et al., 2018b	GEO: GSE102596
Experimental Models: Cell Lines		
585A1	ICSCB	Stem cell ID: SKIP000858
201B7	ICSCB	Stem cell ID: SKIP000001
1231A3	ICSCB	Stem cell ID: HPS0381
CiRA00009	ICSCB	Stem cell ID: SKIP001462
4A6 (4A6C3-10)	Toyohara et al., 2015	N/A
317-12	Oceguera-Yanez et al., 2016	N/A
511-3E	Oceguera-Yanez et al., 2016	N/A
Experimental Models: Organisms/Strains		
NOD.CB17-Prkdcscid/J	Oriental bioservice, Inc	Jackson Laboratory: Stock No: 001303
129S.Cg-Tg(Hoxb7-EGFP)33Cos/J	The Jackson Laboratory	Jackson Laboratory: Stock No: 016251

(*Continued on next page*)

Continued

REAGENT or RESOURCE	SOURCE	IDENTIFIER
Slc:ICR	SHIMIZU Laboratory Supplies Co., Ltd	Jackson Laboratory: Stock No: 009122
Oligonucleotides		
Primers for Figures 1, S1, S2, and S5; Table S4	This paper	N/A
Software and Algorithms		
BZ-X Analyzer	KEYENCE	BZX700
CASAVA 1.8.2	Institut Pasteur	http://bioweb.pasteur.fr/packages/pack@casava@1.8.2
Cell Ranger v2.1.0 pipeline	10X Genomics	https://support.10xgenomics.com/
FACS Diva	BD	FACSDiva v8.0.1 Software
FlowJo	BD	FlowJo v10
ImageJ 1.51u	Schneider et al., 2012	https://imagej.nih.gov/ij/
Microsoft Excel 2013	https://products.office.com/home	Microsoft Office Standard 2013
NIS-Elements AR	Nikon	NIS-Elements AR Ver4.20.00
NIS-Elements Viewer	Nikon	NIS-Elements Viewer Ver. 4.0
R	The R Foundation	R version 3.4.1. or 3.5.2
RPKMforGenes	Sandberg Laboratory	http://sandberg.cmb.ki.se/media/data/rnaseq/instructions-rpkmforgenes.html
RStudio	RStudio, Inc.	RStudio Version 1.1.463
Tophat v2.0.14	Johns Hopkins University	https://ccb.jhu.edu/software/tophat/index.shtml
ZEN 2 blue edition	ZEISS	ZEN 2.3 (blue edition)

LEAD CONTACT AND MATERIALS AVAILABILITY

Further information and requests for resources and reagents should be directed to and will be fulfilled by the Lead Contact, Kenji Osafune (email: osafu@cira.kyoto-u.ac.jp). This study did not generate new unique reagents.

EXPERIMENTAL MODEL AND SUBJECT DETAILS

Human Tissues

Frozen section slides of GW28 human fatal kidney and human adult kidney (78 years old male) were purchased from US Biomax Inc. and BioChain, respectively.

Mice

The Kyoto University Animal Care Committee approved all animal experiments. No formal randomization was performed in this study. Male 5-15 weeks old NOD.CB17-Prkdcscid/J mice were purchased from Oriental bioservice, Inc. All mice were housed at the laboratory animal facility of the Center for iPS Cell Research and Application (CiRA), Kyoto University, under specific pathogen-free (SPF) conditions. The room has controlled temperature (21-25°C), humidity (45%–55%) and light (12-hours light-dark cycle). Mice were provided *ad libitum* access to food and water.

hiPSC Line and Maintenance

Experiments using hiPSCs were approved by the Ethics Committee of Kyoto University, and informed consent was obtained from donors from whom hiPSCs were derived. Two hiPSC lines, 4A6 and 585A1, were maintained on mitomycin C-treated mouse SNL cells in Primate ES medium (ReproCELL) supplemented with 4 ng/ml recombinant human basic fibroblast growth factor (bFGF; Wako) and 500 U/ml penicillin/streptomycin (PS; Thermo Fisher Scientific). For routine passaging, hiPSCs were washed once with phosphate buffered saline (PBS, Nacalai Tesque) and then incubated with CTK dissociation solution containing 0.1% collagenase IV (Thermo Fisher Scientific), 0.25% trypsin (Thermo Fisher Scientific), 20% knockout serum replacement (KSR; Thermo Fisher Scientific) and 1 mM $CaCl_2$ in PBS. The split ratio was between 1:3 and 1:6. hiPSC lines constitutively expressing GFP (317-12) or mCherry (511-3E) along with three other hiPSC lines, 1231A3, 585A1 and CiRA00009, were maintained with feeder-free cultures using Stem Fit AK02N medium (Takara) on cell culture plates coated with iMatrix-511 silk (Nippi). The cells were passaged using 0.5 mM EDTA/PBS (Thermo Fisher Scientific) every four days. hiPSCs were routinely examined for mycoplasma contamination.

METHOD DETAILS

Differentiation Protocols

hiPSC colonies grown on SNL feeder cells were first treated by an enzymatic method with CTK dissociation solution for 3 min to remove SNL cells, dissociated into single cells by gentle pipetting after treatment with Accutase (Innovative Cell Technologies) for 6 min and seeded on Matrigel (Matrigel Matrix Growth Factor Reduced, BD)-coated 24-well plates (CORNING) at a density of 2.5 × 10^4 cells/cm^2 with Primate Repro FF2 medium (ReproCELL), 4 ng/ml bFGF, 10 μM Y-27632 and 500 U/ml PS. On culture day 2, the cells were treated in serum-free differentiation medium consisting of DMEM/F12 Glutamax medium (Thermo Fisher Scientific), B27 supplement minus vitamin A (Thermo Fisher Scientific), and 500 U/ml PS (hereafter called basal medium) supplemented with 1 μM CHIR99021 (StemRD), 10 nM RA (SIGMA), 1 ng/ml BMP4 (Peprotech) and 100 ng/ml bFGF to induce $CDX1^+$ cells.

LPM and vascular cell induction

For differentiation toward LPM and vascular cells, $CDX1^+$ cells were cultured with 3 μM CHIR99021, 100 ng/ml bFGF and 25 ng/ml BMP7 for 3 days. Then, the cells were dissociated with Accutase and replaced on Laminin 411 (BioLamina)-coated 24-well plates in StemPro-34 SFM (Thermo Fisher Scientific) supplemented with 50 ng/ml recombinant human VEGF (Peprotech), 10 ng/ml bFGF, 10 μM DAPT (R&D Systems), 20 ng/ml BMP4 and 10 μM IWR1 (SIGMA) for 4 days.

PAM and sclerotome induction

For differentiation toward PAM and sclerotome, $CDX1^+$ cells were cultured with 3 μM CHIR99021 and 100 ng/ml bFGF. After 12 h, the medium was switched to basal medium containing 3 μM CHIR99021, 100 ng/ml bFGF, 25 ng/ml NOGGIN and 10 μM A83-01 to induce PAM-PS cells. Detailed procedures of the differentiation into PAM and sclerotome were previously described (Nakajima et al., 2018).

IM and metanephric nephron progenitor (NP) induction

For differentiation toward IM and NP cells, $CDX1^+$ cells were cultured with 3 μM CHIR99021, 100 ng/ml bFGF and 1 ng/ml BMP7 (R&D Systems). After 12 h, the medium was switched to basal medium containing 3 μM CHIR99021, 100 ng/ml bFGF, 1 ng/ml BMP7 and 10 μM A83-01 (Wako). At Stage 4, the medium was changed to basal medium containing 3 μM CHIR99021, 100 ng/ml bFGF, 1 ng/ml BMP7, 10 ng/ml activin A (R&D Systems) and 30 μM Y-27632 (Wako). At Stage 5, the medium was changed to basal medium containing 200 ng/ml FGF9 (Peprotech), 0.1 μM RA and 25 ng/ml NOGGIN (Peprotech). At Stage 6, the medium was switched to basal medium containing 200 ng/ml FGF9 and 1 μM CHIR99021. Subsequently, the culture medium was refreshed every day.

Mesonephric NP-like cell induction

The same protocol as the metanephric NP induction described above was used except for removing activin A at Stage 4.

UB induction

UB lineages were induced by modifying a previously reported protocol (Mae et al., 2018). Briefly, hiPSCs were treated with basal medium containing 100 ng/ml activin A, 3 μM CHIR99021 and 10 ng/ml BMP4 for 24 h to induce anterior PS cells. At stage 2, the medium was changed to basal medium containing 200 ng/ml FGF8 (Peprotech), 0.1 μM 4-[(E)-2-(5,6,7,8-Tetrahydro-5,5,8,8-tetramethyl-2-naphthalenyl)-1-propenyl]-benzoic acid (TTNPB; Santa Cruz Biotechnology), 1 μM A83-01 and 0.1 μM LDN193189 for 3 days. Thereafter, anterior IM cells were treated with basal medium containing 1 μM CHIR99021, 0.1 μM LDN193189, 200 ng/ml FGF8 and 100 ng/ml glial cell line-derived neurotrophic factor (GDNF; R&D Systems) for 2 days to enhance WD leading edge cell induction. Then, the cells were reseeded onto low-attachment 96-well plates (Sumitomo Bakelite) at a density of 1 × 10^4 cells/well in basal medium with 100 ng/ml GDNF, 200 ng/ml FGF1 (R&D Systems), 0.1 μM TTNPB, 3 μM CHIR99021 and 10 μM Thiazovivin (Santa Cruz Biotechnology) to induce mature WD aggregates for 2 days. The mature WD aggregates were embedded into 30 μL Matrigel (BD Biosciences) diluted with Essential 6 medium (1:1; Thermo Fisher Scientific) in low-attachment 96-well plates and incubated for 30 min. After the solidification of Matrigel, Essential 6 medium supplemented with 100 ng/ml GDNF, 200 ng/ml FGF1, 0.1 μM TTNPB, 3 μM CHIR99021 and 10 μM Thiazovivin was added.

Immunostaining

The cells were fixed with 4% PFA/PBS at 4°C for 15 min after a brief wash with PBS. Fixed cells were washed with PBS and then blocked with PBST (PBS/0.4% Triton X-100)/5% normal donkey serum (Jackson ImmunoResearch Laboratories, JIRL) for 1 h at room temperature. Whole-mount immunostaining was performed as described previously (Li et al., 2016). In brief, primary antibodies were diluted in blocking solution and incubated with the fixed cells for 3 h at room temperature. After wash with PBST, secondary antibodies were incubated for 30 min at room temperature.

Frozen human embryonic kidney sections (GW28) and human adult kidney sections (78 years old male) were purchased from Biomax and BioChain, respectively. Section immunostaining was started by washing with PBS. Then, the sections were blocked with PBST/5% normal donkey serum for 1 h at room temperature. Primary antibodies were diluted in blocking solution and incubated with the sections for 24 h at 4°C. After wash with PBST, secondary antibodies were incubated for 2 h at 4°C. Information about the antibodies used in this study is shown in Table S3.

Fluorescent images of the reconstructed kidney structures were captured by BZ-X700 (KEYENCE), multiphoton microscopy (Nikon A1R MP) or confocal microscopy (Zeiss LSM710). Image analysis was performed using BZ-X Analyzer (KEYENCE), ZEN 2 blue edition (Zeiss), NIS-Elements Viewer 4.0 (Nikon) or ImageJ version 1.51j8.

Flow Cytometry and Cell Sorting

The cells were incubated with Accumax (Innovative Cell Technologies) for 5 min at 37°C and dissociated by pipetting. Dead cells stained with 4',6-diamidino-2-phenylindole, dihydrochloride (DAPI; 0.1 ng/ml; Thermo Fisher Scientific) were excluded from the analyses. The cells were analyzed and sorted using a FACS Aria II cell sorter (BD). For vascular ECs, anti-FLK1 antibody (359910, BioLegend) and anti-VE-cadherin monoclonal antibody (560410, BD PharMingen) was used at 1:10 and 1:20, respectively. The isolated cells were collected into basal medium containing 10 μM Y-27632. The data were analyzed using the FlowJo or FACS Diva (BD) software programs.

RT-PCR and Real-time Quantitative RT-PCR (qRT-PCR)

Total RNA was isolated using the RNeasy Kit (QIAGEN) according to the manufacturer's recommendations, followed by cDNA synthesis using standard protocols. Briefly, 1 μg of total RNA was treated with DNase I (QIAGEN) for 15 min, and the cDNA was synthesized using ReverTra Ace (TOYOBO) or Superscript III reverse transcriptase (Thermo Fisher Scientific). The cDNA samples were subjected to PCR amplification using a thermal cycler (Veriti 96-well Thermal Cycler; Thermo Fisher Scientific). PCR was performed using the Ex-Taq PCR Kit (Takara) according to the manufacturer's instructions. The PCR cycles were as follows. For *β-ACTIN*, the initial denaturation was performed at 94°C for 2.5 min, followed by 25 cycles of 94°C for 30 s, 60°C for 1 min, 72°C for 30 s and a final extension at 72°C for 10 min. For all other genes, the cycles consisted of an initial denaturation at 94°C for 2.5 min, 30-40 cycles of 94°C for 30 s, 58-62°C for 30 s, 72°C for 30 s and a final extension at 72°C for 7 min. qPCR was performed using the Step One Plus Real-Time PCR System (Thermo Fisher Scientific) and SYBR Green PCR Master Mix (Takara) or using the QuantStudio 12K Flex real-time PCR system (Thermo Fisher Scientific) and Thunderbird SYBR qPCR Mix (TOYOBO). Denaturation was performed at 95°C for 10 min, followed by 45 cycles at 95°C for 5 s and at 60°C for 30 s. As recommended by the manufacturer, the threshold cycle method was used to analyze the data for the gene expression levels and normalized to those of the housekeeping gene, *β-ACTIN*. The PCR reactions were performed in triplicate for each sample. The primer sequences are listed in Table S4.

Tube Formation Assay

The tube formation assay was performed as described previously (Homma et al., 2010). In brief, vascular endothelia derived from hiPSCs were seeded onto Matrigel-coated 24-well plates at 4.0×10^4 cells/well. The cells were incubated for 24 h, and digital images of the tube formation were captured.

Alcian Blue Staining

Cells were fixed with 4% PFA/PBS for 30 min at room temperature, rinsed with PBS and stained overnight with Alcian Blue solution (1% Alcian Blue, pH1; Muto Pure Chemicals).

Organ Culture

Nephron organoid formation was performed as described previously (Li et al., 2016). Briefly, to form cellular aggregates, $OSR1^+SIX2^+$ progenitor cells were sorted by a FACS Aria II and plated in spindle-shaped bottom low adhesion 96-well plates (SUMITOMO BAKELITE) at a density of 1.0×10^5 cells/well with basal medium supplemented with 10 μM Y-27632, 200 ng/ml FGF9 and 1 μM CHIR99021. After 24 h of incubation, the aggregates were transferred onto transwell inserts (Corning) with KR5 medium (DMEM/F12 Glutamax containing 0.1 mM non-essential amino acids (Thermo Fisher Scientific), 500 U/ml PS, 55 μM 2-mercaptoethanol (Thermo Fisher Scientific) and 5% KSR) in the presence of 4.5 μM CHIR99021 and 200 ng/ml FGF2 (Peprotech). After 2 days of culture, the medium was refreshed with KR5 medium, and the aggregates were cultured for an additional 8 days.

Kidney Reconstruction *In Vitro*

For the reconstruction of kidney structures from hiPSC-derived NPs and UB cells, the differentiation protocol for NPs was slightly modified to enhance maturation of the resultant tissues as follows. In brief, hiPSCs cultured under feeder-free conditions were treated with 5 μM CHIR99021 from Stage 2 to Stage 4. Day 8 NPs and day 9 UB tissues were dissociated into single cells by incubation with Accumax at 37°C for 10 min and gentle pipetting. The dissociated single cells were mixed, resuspended in DMEM/F12 Glutamax medium containing 10 μM Y-27632, 100 ng/ml bFGF and 20% KSR and seeded into a 96-well low cell-binding U-bottom plate at 9.0×10^4 NPs and 3.0×10^4 UB cells/well to form aggregates. After 2 days, the formed NP and UB mixed aggregates were transferred onto a transwell insert in DMEM/F12 medium containing 100 ng/ml bFGF and 20% KSR. The plates were agitated using a seesaw shaker (TAITEC). After 2 days, the medium was changed to DMEM/F12 medium containing 20% KSR. The medium was thereafter changed every other day.

Kidney Reconstruction *In Vivo*

Day 8 NPs and day 9 UB tissues were dissociated into single cells by incubation with Accumax at 37°C for 10 min and gentle pipetting. The dissociated single cells were mixed, resuspended in DMEM/F12 Glutamax medium containing 10 μM Y-27632, 100 ng/ml bFGF and 20% KSR and seeded into a 96-well low cell-binding U-bottom plate at 9.0×10^4 NPs and 3.0×10^4 UB cells/well to form aggregates. After 2 days, mixed aggregates were harvested for transplantation.

We slightly modified a previously reported transplantation method (Takebe et al., 2014). After implantation of the mixed kidney progenitor aggregates under kidney capsules of immunodeficient mice, 20 μL Matrigel was inserted to release tension and secure a space for the aggregates (Sharmin et al., 2016). Then, we covered the grafted area with Seprafilm (Kakenseiyaku) to prevent post-surgical adhesion.

Intravital Imaging

Ten days after transplantation, recipient mice were anesthetized with isoflurane. Tail vein injections of 3 mg Hoechst 33342 (Thermo Fisher Scientific) were performed. Host kidney capsules were gently exposed. We observed the transplanted kidney organoids using multiphoton microscopy (Nikon A1R MP). After identification of the grafted organoids, tail vein injections of 2-5 mg Rhodamine B-conjugated dextran (70,000 MW) (Thermo Fisher Scientific) were performed to identify vessel lumens. Microscope-mounted hot plates were used to prevent hypothermia.

QUANTIFICATION AND STATISTICAL ANALYSIS

RNA-seq Data Processing

For bulk RNA sequencing, total RNA was extracted using miRNeasy Mini Kit (QIAGEN). We prepared sequencing libraries using the KAPA Stranded mRNA-Seq Kit (KAPA Biosystems). The libraries were sequenced in 100 cycle Single-Read mode of HiSeq2500. All sequence reads were extracted in FASTQ format using BCL2FASTQ Conversion Software 1.8.4 in the CASAVA 1.8.2 pipeline. The sequence reads were mapped to hg19 reference genes using Tophat v2.0.14 and were normalized and quantified using RPKMforGenes, downloaded on 10 December 2012. Gene expression levels were represented by log2(RPKM+1). A heatmap of the gene expressions was generated by the heatmap.2 function of the gplots 3.0.1 library in R 3.4.1. Hierarchal clustering was conducted according to a previous report (Takasato et al., 2015).

Single-cell RNA-seq Data Processing

For single cell RNA sequencing, the isolation of single cells and preparation of a library with cell barcodes were conducted using the ddSEQ platform (Bio-Rad Laboratories) and SureCell WTA 3′ Library Prep Kit (Illumina). Sequencing was performed on an HiSeq2500 with paired 68-bp and 75-bp reads. Demultiplexing and conversion of BCL base call files to FASTQ format from BCL files were performed using bcl2fastq v2.20.0.422. Alignment to the human reference genome hg19, filtering, debarcoding and UMI counting were conducted using the Cell Ranger v2.1.0 pipeline (10X Genomics).

Image Quantification for %SIX2 (+) Cells

Day 11 NPs were dissociated and plated in flat-bottom 24-well plates (Greiner) at a density of 2.0×10^5 cells/well with basal medium supplemented with 10 μM Y-27632, 200 ng/ml FGF9 and 1 μM CHIR99021. After 24 h of incubation, the cells were fixed with 4% PFA/PBS at room temperature for 15 min after a brief wash with PBS. Fixed cells were washed with PBS and then blocked with PBST/5% normal donkey serum for 1 h at room temperature. The cells were then immunostained with SIX2 antibody and DAPI. Images were captured at nine images per well by using BZ-X700 and analyzed with the analyze particle function (ImageJ) for (%) SIX2 (+) cells by calculating the total number of SIX2(+) cells/DAPI(+) cells. The protocol for the image analysis was optimized using day 6 posterior PS cells and day 11 NPs derived from an OSR1-GFP/SIX2-tdTomato reporter hiPSC line as negative and positive controls, respectively.

Statistical Analysis

Data are expressed as the mean ± SEM. Student's t tests were performed to compare the mean values when the experimental design was composed of two individual groups. One-way ANOVA and Bonferroni's post hoc test (Figure S2I) or Tukey-Kramer post hoc test (Table S3) were used for multiple group comparisons. Significant differences are labeled in the figures as $^*p < 0.05$, $^{**}p < 0.01$, and $^{***}p < 0.001$.

DATA AND CODE AVAILABILITY

The NCBI GEO accession number for the RNA sequencing data reported in this paper is GSE146119.